AWARD NUMBER: W81XWH-11-1-0372

TITLE: Intracellular Protein Delivery for Treating Breast Cancer

PRINCIPAL INVESTIGATOR: Pin Wang

CONTRACTING ORGANIZATION: University of Southern California
Los Angeles, CA 90089-0701

REPORT DATE: August 2014

TYPE OF REPORT: Final Report

PREPARED FOR: U.S. Army Medical Research and Materiel Command
Fort Detrick, Maryland 21702-5012

REPORT DOCUMENTATION PAGE

Form Approved
OMB No. 0704-0188

1. REPORT DATE	2. REPORT TYPE	3. DATES COVERED
August 2014	Final	15 May 2011 to 14 May 2014

4. TITLE AND SUBTITLE
Intracellular Protein Delivery for Treating Breast Cancer

5a. CONTRACT NUMBER

5b. GRANT NUMBER
W81XWH-11-1-0372

5c. PROGRAM ELEMENT NUMBER

6. AUTHOR(S)
Pin Wang

E-Mail: pinwang@usc.edu

5d. PROJECT NUMBER

5e. TASK NUMBER

5f. WORK UNIT NUMBER

7. PERFORMING ORGANIZATION NAME(S) AND ADDRESS(ES)
University of Southern California

Los Angeles, CA 90089-0701

8. PERFORMING ORGANIZATION REPORT NUMBER

9. SPONSORING / MONITORING AGENCY NAME(S) AND ADDRESS(ES)

U.S. Army Medical Research and Materiel Command
Fort Detrick, Maryland 21702-5012

10. SPONSOR/MONITOR'S ACRONYM(S)

11. SPONSOR/MONITOR'S REPORT NUMBER(S)

12. DISTRIBUTION / AVAILABILITY STATEMENT

Approved for Public Release; Distribution Unlimited

13. SUPPLEMENTARY NOTES

14. ABSTRACT

Encapsulating anticancer protein therapeutics in nanocarriers is an attractive option to minimize active drug destruction, increase local accumulation at disease site and decrease side effects to other tissues. In this final report, we summarize major accomplishments for the study of polymeric nanocapsulses for delivering protein drugs apoptin and p53. We succeeded in synthesizing degradable, core-shell apoptin and p53 nanocapsules. Recombinant apoptin was reversibly encapsulated in a positively charged, water soluble polyermic shell and is released in native forms in responses to reducing conditions such as the cytoplasm. Rationally designed non-covalent protein nanocapsules, incorporating copper-free click chemistry moiety, PEG unit, redox-sensitive crosslinker, and tumor specific targeting ligand, were synthesized and were shown to selectively deliver intracellular p53 into tumor cells. The study validate a general approach for protein delivery into tumor cells for breast cancer treatment.

15. SUBJECT TERMS
Nanocapsules, Nanoparticles, Apoptin, Breast Cancer, Targeted Delivery, Nanomedicine, Nanogel, Redox-responsive, Apoptosis, p53

16. SECURITY CLASSIFICATION OF:			17. LIMITATION OF ABSTRACT	18. NUMBER OF PAGES	19a. NAME OF RESPONSIBLE PERSON
a. REPORT	b. ABSTRACT	c. THIS PAGE			USAMRMC
U	U	U	UU	40	19b. TELEPHONE NUMBER *(include area code)*

Table of Contents

Page

1. INTRODUCTION

Specific induction of cell death in tumors is considered one of the most desired and effective anticancer therapies. Effective strategies to activate the apoptotic pathway, or other death mechanisms, are currently being intensely pursued. A potent chemotherapy option is directly arming the cancer cells with executioner proteins or apoptotic-inducing proteins that are not targeted by anti-apoptotic maneuvers found in many tumors. In this proposal, we will develop a new method to treat breast cancer by using a native-protein delivery approach. This is a platform to deliver proteins in native forms into cells. The key design feature of our strategy is to first encapsulate protein molecules in a thin layer of water soluble, positively charged, degradable polymer to form nanometer-sized nanocapsules. The nanocapsule shell facilitates uptake of the protein content into cells, and protects the protein both during in vivo circulation and endocytosis. To endow the nanocapsules biodegradability once entered the target cells, the polymer shell is crosslinked with redox-sensitive crosslinkers that can be reduced upon encountering the reducing environment of the cytoplasm. Our overall research objective is to thoroughly evaluate this delivery method as a potentially new therapeutic modality for breast cancer treatment. Three aims will be pursued in parallel and results from each aim will be used to guide the refinement of other aims and the overall research objective. 1) Delivering different target proteins to breast cancer cell lines using this approach, including the tumor specific apoptin; 2) Equipping the protein nanocapsules with specific cancer cell targeting ligands; 3) Examining the in vivo potency and pharmacokinetics of the nanocapsules.

2. KEYWORDS

Nanocapsules, Nanoparticles, Apoptin, Breast Cancer, Targeted Delivery, Nanomedicine, Nanogel, Redox-responsive, Apoptosis, p53

3. ACCOMPLISHMENTS

Background and Motivation

Intracelluar delivery of recombinant proteins for cancer therapy The most desirable cancer therapy is both potent and specific towards tumor cells (Atkins and Gershell, 2002; Gibbs, 2000). Many conventional small molecule chemotheraputics do not discriminate between cancerous and normal cells, cause undesirable damage to healthy tissues, and are therefore unable to be administered at high dosage. In contrast, cytoplasmic and nuclear proteins that selectively alter the signaling pathways in tumor cells, reactivate apoptosis and restore tissue homeostasis, can eradicate cancerous cells and delay tumor progression with less collateral damage to other tissues (Cotter, 2009; Evan and Vousden, 2001; Reed, 2003). Intracellular delivery of such proteins, including human tumor suppressors (such as p53) (Brown et al., 2009) and exogenous tumor-killing proteins (such as apoptin) (Backendorf et al., 2008), in their functional forms is attractive as a new anti-cancer therapy modality.

Apoptin Apoptin is a small protein (121 amino acids) from chicken anemia virus (CAV) that induces p53-independent apoptosis in a tumor-specific way (Backendorf et al., 2008). In a variety of tumor cell lines, Apoptin becomes phosphorylated, enters the nucleus, and induces apoptosis (Danen-Van Oorschot et al., 1997; Danen-Van Oorschot et al., 2003; Zhuang et al., 1995). In sharp contrast, Apoptin is unphosphorylated in normal cells and stays in the cytoplasm. An important feature of Apoptin is that it can recognize early stages of oncogenesis and it can induce apoptosis. Currently known Apoptin targets include DEDAF, Nur77, Nmi, and Hippi, some of which are p53-independent signaling proteins in the apoptotic pathway (Backendorf et al., 2008). Due to its high selectivity and potency, Apoptin has become an attractive antitumor target for gene therapy approaches. For example, in a nude mouse model, injection of Apoptin-encoding adenoviruses to the site of breast carcinoma xenografts resulted in a significant reduction in tumor growth. Furthermore, Apoptin has been shown to be a safe agent, resulting in minimal toxicity and weight loss in mouse models. Recombinant Apoptin expressed by *E. coli* can induce rapid apoptosis in cancer cells when microinjected into tumor cells (Leliveld et al., 2003). In comparison, no apoptosis was observed in normal cells. Moreover, when fused to the HIV-TAT protein transduction domain, TAT-Apoptin was transduced efficiently into normal and

tumor cells. However, TAT-Apoptin remained in the cytoplasm and did not kill normal 6689 and 1BR3 fibroblasts. In contrast, TAT-Apoptin migrated from the cytoplasm to the nucleus of Saos-2 and HSC-3 cancer cells resulting in apoptosis after 24 h (Guelen et al., 2004). These results indicate that recombinant Apoptin captures all of the essential functions and selectivity of the native protein. Therefore, Apoptin is an excellent target for expanding the applications of nanocapsules as a chemotherapy modality.

p53 and its delivery Virtually all human cancer cells have elaborate anti-apoptotic strategies to overcome apoptosis, which is a vital cellular mechanism to obstruct tumor progression (Cotter, 2009). The most commonly mutated gene in tumor cells is the tumor suppressor gene TP53, the protein product of which promotes apoptosis of aberrant cells through both transcription-dependent and independent mechanisms (Coles et al., 1992). In this manner, the genome guardian p53 is critically important in eliminating possible neoplastic cells incurred during DNA damage. About 50% of all the human tumors have mutant p53 proteins (Lacroix et al., 2006). Therefore, restoring p53 function can be a highly effective option for cancer treatment. Functional copies of p53 can not only resurrect the apoptotic circuitry, but also sensitize the tumor cells towards other various treatments (radio- and chemotherapy) (Blagosklonny, 2002). Different strategies pursuing this goal have been intensively investigated, including small molecules and peptides that overcome p53 mutations, as well as adenovirus/p53 gene delivery vectors (Friedler et al., 2002; Issaeva et al., 2004; Senzer et al., 2007; Vassilev et al., 2004). While restoring p53 functions in cancer cells has been a tantalizing approach towards combating cancer, the lack of effective delivery method has undermined its potential as an anti-cancer therapeutic. Intracellular protein delivery using stimuli-responsive nanomaterials has emerged as an attractive method to deliver various cargos to the cells of interest (Cho et al., 2012; Chorny et al., 2010; Giannotti et al., 2011; Hu et al., 2009; Lee et al., 2009; Liechty et al., 2009). In particular, water-soluble polymer-based nanocarriers that encapsulate the protein of interest to aid the penetration of cellular membrane, while capable of releasing the protein upon various cellular stimuli, have been demonstrated to be effective in functional delivery of proteins (Gu et al., 2011). Nanocarriers that can be triggered to release protein cargo in response to changes in temperature, light, pH, redox potential and enzymatic activities have been reported (Lee et al., 2009; Zhao et al., 2011). As a result, nanocapsules-mediated delivery of recombinant p53 to cancer cells may be a direct method of reactivating the apoptosis pathway and inducing programmed cell death.

Specific Aim 1: Delivering Different Target Proteins to Breast Cancer Cell Line Using Protein Nanocapsules

Synthesis and characterization of apoptin nanocapsules In this study, we aimed to test the polymeric nanocapsule (NC) strategy for the functional delivery of recombinant maltose-binding-protein-fused apoptin (MBP-APO), in which the protein complex is noncovalently protected in a water-soluble polymer shell (Figure 1a). MBP-APO (pI = 6.5) was first purified from *E. coli* extract using an amylose-affinity column. Dynamic light scattering (DLS) measurement revealed an average hydrodynamic radius of 36.1nm, consistent with the reported size for the recombinant MBP-APO complex (Leliveld et al., 2003). Transmission electron microscopy (TEM) analysis of MBP-APO showed similarly sized protein complexes (Fig. 1c and enlarged in Fig 1d). Interestingly, MBP-APO complexes appear to adopt a diskshaped structure despite the lack of defined secondary structure from the apoptin component. Since the apoptin portion of the protein can self-assemble into the ~40-mer complex, we propose a three dimensional arrangement of MBP-APO in which the C-terminal apoptin forms the central spoke of the wheel-like structure (Fig. 1a), with the larger MBP portion distributes around the apoptin. The planar arrangement allows the apoptin portion of the fusion protein to remain accessible to its protein partners, which may explain how the MBP-APO fusion retains essentially all of the observed functions of native apoptin.

The reversible encapsulation strategy for producing apoptin NCs is shown in Fig. 1a. Following electrostatic deposition of the monomers acrylamide (**1** in Fig. 1a) and N-(3-aminopropyl)methacrylamide (**2**), and the crosslinker N,N-bis(acryloyl)cystamine (**3**), at a molar ratio of 1.5:1:0.14, onto MBP-APO (1 mg) in carbonate buffer (5 mM, pH 9.0), in situ polymerization was initiated with the addition of free radical initiators and proceeded for 1 h. The molar ratio and the time of reaction reported were optimized to minimize protein aggregation and precipitation, as well as to maximize the solution stability of the resulting NCs (designated below as S-S APO NC). Excess monomers and cross-linkers were removed using ultrafiltration and S-S APO

NC was stored in PBS buffer (pH 7.4). DLS clearly showed increase in average diameter of the sample to ~75nm with a slightly positive-potential value of 2.8mV. TEM analysis of the S-S APO NC confirmed the nearly doubling in diameter of the spherical particle (Fig. 1e). Unexpectedly, the NCs displayed dark contrast upon uranyl acetate staining, which hints that the cores of the particles were very densely packed. As expected from the incorporation of redox-responsive cross-linker **3**, the reduction of NCs size can be seen upon treatment of the reducing agent glutathione (GSH) (2 mM, 6 h, 37 ◦C). As shown in Fig. 1f, the densely packed NCs were completely dissociated into ~30nm particles, confirming the reversible nature of the encapsulation process. As a control, we also synthesized nondegradable MBP-APO NCs (ND APO NC) using N,N-methylene bisacrylamide as the cross-linker with same monomer and protein concentrations under identical reaction conditions. Whereas similarly sized NCs were formed, no degradation of ND APO NC can be observed in the presence of GSH.

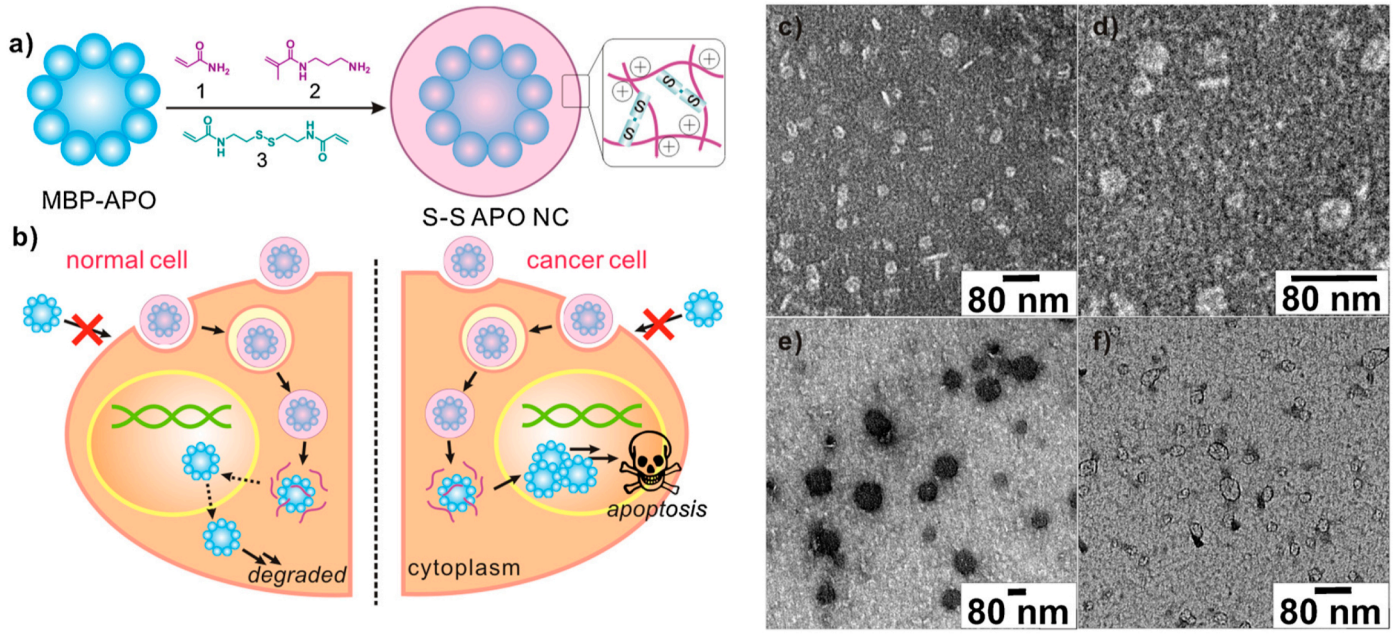

Figure 1: Degradable nanocapsules for apoptin delivery. (a &b) Schematic diagram of synthesis of degradable apoptin nanocapsules (S-S APO NC) and delivery into tumor cells to induce apoptosis; TEM images of (c) native MBP-APO; (d) enlarged image of MBP-APO; (e) S-S APO NC; and (f) degraded S-S APO NC after treatment with 2 mM GSH for 6 h at 37 °C.

Synthesis and characterization of p53 nanocapsules The strategy for synthesis of p53 nanocapsule is shown in Figure 2a. Monomers and redox-sensitive crosslinkers can deposited at the surface of the target protein via van der Waals interactions, and can be polymerized in situ around the target protein to form a non-covalent shell that encapsulates the protein. The monomer acrylamide (**1**) is used as a general building block of the water-soluble shell. The nanocapsules are crosslinked with N,N-bis(acryloyl)cystamine, which is designed to degrade in highly reducing environments such as the cytoplasm, thereby releasing the protein cargo intracellularly. To synthesize a near-neutral polymer shell that does not enter cells via positive charges, we first eliminated the use of positively charged monomers employed in previous designs. Instead, we chose N-(azidoethyl-decaethylene glycol)-acrylamide (**2**) as the second monomer (Figure 2a). The neutral **2** contains a terminal azido group that can be used as the reactive site for cross-coupling via copper-free click reaction. The ten ethylene glycol units serve as a water-soluble spacer at the surface of the nanocapsules, and provide flexibility to the conjugated targeting ligands. Through copolymerization of **1** and **2**, the azido functionalities can be displayed on the surface of the nanocapsules for subsequent modification. Monomer **2** was readily prepared by reacting O-(2-aminoethyl)-O-(2-asidoethyl)nonaethylene glycol with acryloyl chloride. After purification and MS characterization of monomer **2**, we first performed the in situ polymerization process using GFP as the cargo. Following one hour of polymerization during which the mole fraction of **2** was 1.5% of total monomers, uniformly sized nanocapsules were synthesized, with an electrostatic potential of ~0.9 mV, and an average size of 9.1 nm. To examine the structural integrity of the encapsulated proteins, we performed circular

dichroism measurement on both free GFP and GFP-containing nanocapsules. As expected, no significant change to the secondary structure of GFP was observed upon encapsulation.

To verify the presence of azido groups on the surface of the nanocapsules, we performed the copper-free reaction between dibenzylcyclooctyne TAMRA (DBCO TAMRA, **4**) and the GFP nanocapsules prepared from monomers **1** and **2**. As a control, nanocapsules synthesized from **1** alone were also mixed with **4**. After overnight stirring at 4 °C, the reaction was subjected to repeated dialysis and ultracentrifugation to remove any unreacted **4**. The conjugation of TAMRA to the protein nanocapsules was detected by fluorescence emission scan (Figure 2b). Whereas nanocapsules synthesized with both **1** and **2** exhibited the characteristic emission peak at 580 nm of TAMRA, the control sample with only **1** showed nearly no additional signal at the same wavelength compared to negative controls. Given the measured differences in hydrodynamic radius between the GFP nanocapsules (4.5 nm) and free GFP (2.5 nm), we estimate no more than three GFP can be packed into each nanocapsule. We previously established by experiments that more the nanocapsules prepared via the interfacial polymerization method contain a single copy of GFP. Taking together, the nanocapsules synthesized in this study should contain either one or two GFP molecules. The number of TAMRA molecules conjugated per nanocapsule was approximated by comparing of relative intensities of GFP and TAMRA fluorescence. Given the above estimation of one to two GFP per nanocapsule, we approximated that each

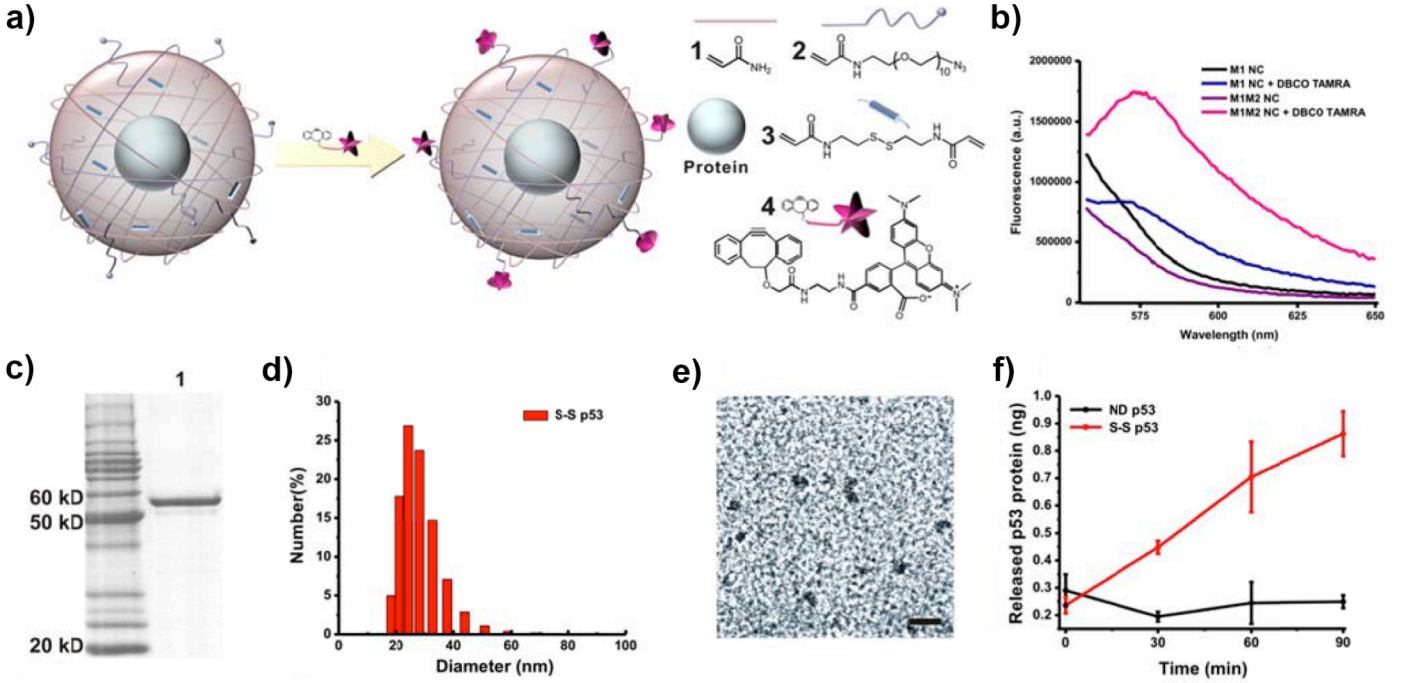

Figure 2: Clickable nanocapsules. **a**) Schematic diagram of clickable, redox-sensitive protein nanocapsules, and the scheme of conjugation to DBCO TAMRA using copper-free click chemistry. **b**) Fluroscence spectra of GFP NC samples before and after copper-free click conjugation to DBCO TAMRA. **c**) SDS-PAGE of refolded p53 protein. **d**) The hydrodynamic size distribution of S-S p53 NC as measured by DLS. **e**) TEM image of S-S p53 NC. The scale bar represents 50 nm. **f**) ELISA assay measuring p53 released from S-S p53 NC and ND p53 NC after treatment with 2 mM DTT over 90 min at 37 °C (n=2).

nanocapsule was conjugated with four to eight TAMRA molecules through the click reaction with accessible azido functional groups.

After the establishment of nanocapsule synthesis using GFP as a model protein, we then applied this method to make p53 nanocapsules. Delivery of recombinant p53 poses significant challenges as the tetrameric complex can readily aggregate and lose activity under non-native condition. The three-dimensional structure of p53 is also not well resolved, and has been shown to be loosely organized, especially in the absence of DNA. Recombinant p53 was expressed in E. coli, purified from inclusion bodies and refolded as soluble tetrameric protein (Figure 2c). The in situ polymerization process using monomers **1** and **2**, as well as crosslinker **3** was optimized to minimize aggregation and precipitation of the soluble p53. A final molar fraction of 1.5% of **2** was used in the monomers, while 5% 3 was added as crosslinkers. We found that p53 concentration must be kept

at below 0.7 mg/mL and all steps must be performed in sodium bicarbonate containing buffer to avoid aggregation and precipitation. After encapsulation, the azido-functionalized nanocapsules (S-S p53 NC) were buffer-exchanged and concentrated in PBS. Successful encapsulation was monitored by both DLS and TEM as shown in Figure 2d and Figure 2e, respectively. The native p53 tetramer exhibited hydrodynamic diameter of 7.7 nm, in line with cryo-EM characterizations. Upon encapsulation, the average diameter increased to ~27.5 nm with a zeta-potential of 0.6 mV, and the structural uniformity was observed by TEM. As a nondegradable control, p53-containing nanocapsules crosslinked with the N,N-methylene bisacrylamide was also prepared. The physical properties of the azido-functionalized nano-degradable p53 nanocapsules (ND p53 NC) were nearly identical to that of the S-S p53 NCs.

To examine the encapsulation effectiveness and redox-sensitive release of the p53 nanocapsules, we performed time-dependent ELISA analysis of p53 nanocapsules both in the presence and absence of the reducing agent DTT (Figure 2f). The ELISA assay employed here requires the p53 to bind to a specific, double stranded target oligonucleotide immobilized on strip well plates. Therefore, encapsulated p53 is physically shielded by the polymer layer and is thus unable to bind to oligonucleotide and to be recognized by the anti-p53 antibody. As expected in the absence of DTT, no native p53 in the solution can be detected within the assay period, indicating the robustness of the polymer layer in both shielding and retaining the p53 cargo. In contrast, the S-S p53 NCs released p53 when 2 mM DTT was added to the nanocapsules, indicating degradation of the crossliner and release of p53 into the solution. The positive ELISA signal also signifies that the p53 protein subjected to encapsulation and release remained functional. The ND p53 NCs control did not release detectable p53 in the presence of 2 mM DTT, further confirming the redox-responsiveness of the S-S p53 NCs.

Functional studies of apoptin nanocapsules in vitro After the successful synthesis of apoptin nanocapsules, we examined the cellular uptake of the S-S APO NC and cellular localization of the cargo. If the unique tumor selectivity of MBP-APO is maintained following the encapsulation and release processes, we expect the delivered MBP-APO to either accumulate in the nuclei of the tumor cells, or to localize in the cytoplasm of noncancerous cells. Prior to the polymerization process, the MBP-APO protein was conjugated to amine-reactive rhodamine (Rho-APO). Subsequent encapsulation yielded similarly sized NCs as unlabeled S-S APO NCs. Fluorescent microscopy showed all NCs readily penetrated the cell membrane and are present in the cytoplasm of MDA-MB-231 cells within 1 h. When the relative amounts of positively charged monomer were reduced in the NC shell, corresponding decreases in zeta-potentials of the NCs were measured by DLS, which led to decreases in cellular internalization. The cellular trafficking of the internalized S-S Rho-APO NCs in HeLa cells was investigated for 2 h by monitoring colocalization using fluorescent markers for early and late endosomes. Colocalization of Rho-APO with early endosomes was detected at the highest levels after 30 min and decreased at later time points. In contrast, colocalization of Rho-APO with late endosome remained low throughout the trafficking studies. Colocalization of Rho-APO with nuclei became evident after 2 h, indicating endosomal escape and nuclear entry of the released apoptin protein. These results suggested that S S Rho-APO NCs were trafficked into early endosomes upon internalization and at least a significant portion of the

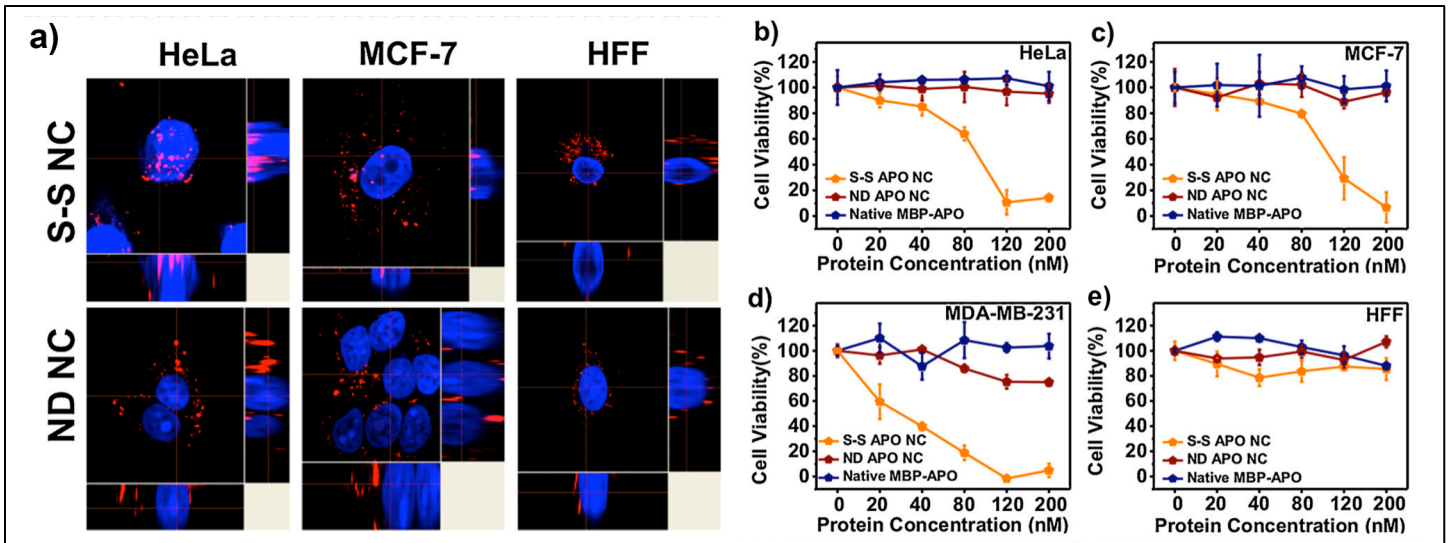

Figure 3: (a) Confocal microscopy of cellular localization of Rho-APO encapsulated in S-S NC and ND NC to cancer cell lines HeLa and MCF-7, and noncancerous HFF. Nuclei were stained with DAPI (blue). (b-e) HeLa (b), MCF-7 (c), MDA-MB-231 (d), or HFF (e) cells were treated with various concentrations of S-S APO NC, ND APO NC, and native MBP-APO. Cell viability was measured by a XTT assay.

internalized NCs and the cargo can escape from the endosomal compartment.

To analyze protein localization using confocal microscopy, two cancer cell lines HeLa and MCF-7, together with the noncancerous human foreskin fibroblast (HFF), were treated with either S-S Rho-APO NC or ND Rho-APO NC (Figure 3a). In the case of ND Rho-APO NCs, red fluorescence signals remained in the cytoplasm for all three cell lines, indicating the encapsulated Rho-APO proteins were well-shielded by the nondegradable polymer shell and the internal nuclear localization sequences were not accessible to the transport machinery. In stark contrast, when HeLa cells were treated with S-S Rho-APO NC, strong red fluorescence of rhodamine was present in the nuclei, resulting in intense pink color as a result of overlapping of rhodamine and DAPI fluorescence. Z-stacking analysis confirmed the Rho-APO to be localized inside of the nuclei. Similar results were observed with MCF-7 cells, although the fluorescence intensity was not as strong as in the HeLa cells. These results confirmed that the Rho-APO delivered can indeed be released in native forms inside the cytoplasm and enter the nuclei. More importantly, the tumor-specificity of delivered apoptin proteins toward cancer cell lines were demonstrated in the confocal analysis of noncancerous HFF cells treated with S-S Rho-APO NC, as all of the dye signals remained in the cytoplasm and no nuclear accumulation was observed.

We then investigated whether the MBP-APO protein delivered still possesses its function to induce tumor-selective apoptosis. The potency and selectivity of S-S APO NC were tested on various cell lines including HeLa, MCF-7, MDA-MB-231, and HFF (Figures 3b-3e). MTS assay was used to measure cell viability 48 h after addition of the protein and NC. For each cell line, ND APO NC and native MBP-APO were used as negative controls. When S-S APO NC was added to a final concentration of 200 nM, all three cancer cell lines had no viable cells, whereas ~75% of the HFF had survived. The IC50 values were 80 and 30 nM for HeLa and MDA-MB-231, respectively. The IC50 for MCF-7 was higher at ~110 nM, which may be due to the deficiency in the terminal executioner caspase 3 and reliance on other effector caspases for apoptosis. As expected, native MBP-APO and ND APO NC did not significantly decrease the viability of any cell lines tested, consistent with the inability to enter cells and release MBP-APO in cytoplasm, respectively. The IC50 values of S-S APO NC toward MDA-MB-231 increased as the surface charge of the NC became more neutral, suggesting more efficient internalization can improve S-S NCs cytotoxicity. The morphologies of MDA-MB-231 and HFF cells were examined under various treatments. Only the S-S APO NC treated MDA-MB-231 cells exhibited blebbing and shrinkage, which are hallmarks of apoptotic cell death. Using TUNEL assay, S-S APO NC treated MDA-MB-231 also showed nuclear fragmentation associated with apoptosis, whereas cells treated with native MBP-APO and ND APO NC at the same concentration, as well as HFF treated with 200 nM S-S APO NC, had no sign of apoptosis. Collectively, these results demonstrated that the recombinant MBP-APO delivered by the degradable NCs retains the potency and selectivity.

Specific Aim 2: Equipping Protein Nanocapsules with Specific Cancer Cell Targeting Ligands

iRGD-conjugated Nanoparticles As we are working on the design of targeting strategies for nanocapsules, new progress has emerged from the field. As we all know that one of major obstacle for nanoparticle-based drug delivery is the poor penetration of the targeted payload through the vascular wall and into the tumor parenchyma, especially in solid tumors, which have a high interstitial pressure (Heldin et al., 2004; Jain, 1999). To address this challenge, a tumor-penetrating peptide, iRGD, was identified and reported to increase vascular and tissue penetration in a tumor-specific and neuropilin-1-dependent manner, as compared to the conventional RGD peptides (Sugahara et al., 2009; Sugahara et al., 2010). Like conventional RGD peptides, iRGD homes to tumor sites by binding to $\alpha_v\beta_3$ and $\alpha_v\beta_5$ integrins, which are highly expressed in tumor endothelium (Mitra et al., 2005; Murphy et al., 2008; Sugahara et al., 2009), thus enhancing the therapeutic effect of antitumor drugs on suppressing tumor growth and/or metastasis. After binding, the iRGD peptide is thought to be proteolytically cleaved to produce CRGDK fragment, which favors binding to neuropilin-1 receptor, thus facilitating the penetration of drugs into the tumor (Feron, 2010). Thus, we explored whether the iRGD peptide could improve the nanoparticle delivery. As a proof of concept, our work initially focused on the crosslinked multilamellar liposomal vesicle (cMLV)-based nanoparticles as a model system to test the assays and biological efficacy, which can be directly translated into nanocapsules.

Preparation of liposomes was based on the conventional dehydration-rehydration method. All lipids were obtained from NOF Corporation (Japan). 1.5 μmol of lipids 1,2-dioleoyl-sn-glycero-3-phosphocholine

(DOPC), 1,2-dioleoyl-sn-glycero-3-phospho-(1'-rac-glycerol) (DOPG), and maleimide-headgroup lipid 1,2-dioleoyl-sn-glycero-3-phosphoeth-anolamine-N-[4-(p-maleimidophenyl) butyramide (MPB-PE) were mixed in chloroform to form a lipid composition with a molar ratio of DOPC:DOPG:MPB = 4:1:5, and the organic solvent in the lipid mixture was evaporated under argon gas, followed by additional drying under vacuum overnight to form dried thin lipid films. The resultant dried film was hydrated in 10 mM Bis-Tris propane at pH 7.0 with doxorubicin at a molar ratio of 0.2:1 (drugs:lipids) with vigorous vortexing every 10 min for 1 h and then applied with 4 cycles of 15-s sonication (Misonix Microson XL2000, Farmingdale, NY) on ice at 1 min intervals for each cycle. To induce divalent-triggered vesicle fusion, $MgCl_2$ was added to make a final concentration of 10 mM. The resulting multilamellar vesicles were further crosslinked by addition of dithiothreitol (DTT, Sigma-Aldrich) at a final concentration of 1.5 mM for 1 h at 37°C. The resulting vesicles were collected by centrifugation at 14,000 g for 4 min and then washed twice with PBS. For iRGD conjugation to cMLVs, the particles were incubated with 0.5 μmol of iRGD peptides (GenScript, Piscataway, NJ) for 1 h at 37°C. For pegylation of cMLVs, both unconjugated and iRGD-conjugated particles were further incubated with 0.5 μmol of 2 kDa PEG-SH (Laysan Bio Inc., Arab, AL) for 1 h at 37°C. The particles were then centrifuged and washed twice with PBS. The final products were stored in PBS at 4°C. The hydrodynamic size and size distribution of iRGD-NPs were measured by dynamic light scattering (Wyatt Technology, Santa Barbara, CA). The hydrodynamic size of these targeted nanoparticles was measured by dynamic light scattering (DLS), and the result showed the mean diameter of iRGD-NPs to be ~230 ± 11.23 nm, which was similar to that of unconjugated cMLV (~220 ± 6.98 nm). To examine whether iRGD peptides were conjugated to the surface of nanoparticles via the maleimide headgroups, fluorescent 1,1-dioctadecyl-3,3,3,3-tetramethylindodicarbocyanine (DiD)-labeled nanoparticles were used to visualize both unconjugated and conjugated particles. In addition, Alexa488 dye was utilized to label iRGD peptides through the amine group of lysine residues on iRGD peptides (CRGD**K**GPDC). The results showed that a significant colocalization of DiD-labeled iRGD-NPs with Alexa488-labeled iRGD peptides was observed, while no Alexa488 signals were detected on unconjugated particles, suggesting that iRGD peptides were successfully conjugated to nanoparticles.

Internalization and intracellular pathways of iRGD-cMLVs We next investigated the entry mechanism and intracellular process of iRGD-NPs into tumor cells to determine whether iRGD peptides could change the pathway by which nanoparticles are endocytosed. Endocytosis is known as one of the main entry mechanisms for various nanoscale drug carriers (Dobson and Kell, 2008; Petros and DeSimone, 2010). Several studies have reported the involvement of clathrin- and caveolin-dependent pathways in nanoparticle-mediated endocytosis (Conner and Schmid, 2003; Le Roy and Wrana, 2005; Pelkmans and Helenius, 2002). Therefore, to investigate the role of clathrin- or caveolin-dependent endocytosis of iRGD-NPs, we visualized the individual fluorescent DiD-labeled NPs or iRGD-NPs with endocytic structures (clathrin or caveolin) after 15 min incubation at 37°C. As shown in Figure 4a, a significant colocalization of unconjugated nanoparticles with caveolin-1 signals was observed, while no colocalization between unconjugated nanoparticles and clathrin structures was detected, indicating that the caveolin pathway may be involved in the endocytosis. However, after 15 min incubation, iRGD-NPs were colocalized with clathrin structures, whereas, no significant colocalization between iRGD-NPs and caveolin-1 signals was observed (Figure 4b), suggesting that the endocytosis of iRGD-NPs could be clathrin-dependent. The quantification of iRGD-NPs and NPs colocalized with caveolin-1 or clathrin structures by analyzing more than 30 cells confirmed that the clathrin-mediated pathway could be involved in the entry of iRGD-NPs, while the endocytosis of NPs could be caveolin-1-dependent (Figure 4c and 4d). The role of clathrin-dependent endocytosis of iRGD-NPs was further examined by drug-inhibition assays shown in Figure 2E. Chlorpromazine (CPZ) is known to block clathrin-mediated internalization by inhibiting clathrin polymerization (Wang et al., 1993), while filipin is a cholesterol-binding reagent that can disrupt caveolin-dependent internalization (Neufeld et al., 1996; Rothberg et al., 1992). As shown in Figure 4e, CPZ (10 μg/ml) significantly decreased the uptake of iRGD-NPs in HeLa cells, while no significant inhibitory effect on their uptake was observed when cells were pretreated with Filipin (10 μg/ml). However, pretreatment of cells with Filipin remarkably decreased the uptake of unconjugated nanoparticles ($P < 0.01$), whereas no inhibitory effect on their uptake was observed in CPZ-pretreated cells. Results from the inhibition assay further confirmed that iRGD-NP endocytosis is mediated by the clathrin-dependent pathway, while unconjugated particles enter cells via caveolin-dependent endocytosis.

Once inside the cells, the intracellular fate of the endosomal contents has been considered as an important determinant of successful drug delivery (Bareford and Swaan, 2007). It was also proposed that nanoparticles might transport to the early endosomes in a GTPase Rb5-dependent manner and also proceed

through the conventional endocytic pathway (endosomes/lysosomes) (Carlsson et al., 1988; Christoforidis et al., 1999; Luzio et al., 1990), probably resulting in enzymatic destruction of lipid membrane for drug release in lysosomes (Bareford and Swaan, 2007). To further investigate the subsequent intracellular fate of iRGD-NPs, DiD-labeled iRGD-NPs were evaluated for their colocalization with the early endosome (EEA-1) (Pelkmans et al., 2001) and lysosome (Lamp-1) (Carlsson et al., 1988) markers at different incubation times at 37°C. Most iRGD-NPs were found in the $EEA1^{+}$ early endosomes after incubation of 30 min, validating the involvement of early endosomes in the intracellular fate of targeted nanoparticles. In addition, after 2h incubation, a significant colocalization of iRGD-NPs with lysosomes was observed, suggesting that iRGD-NPs may transport to early

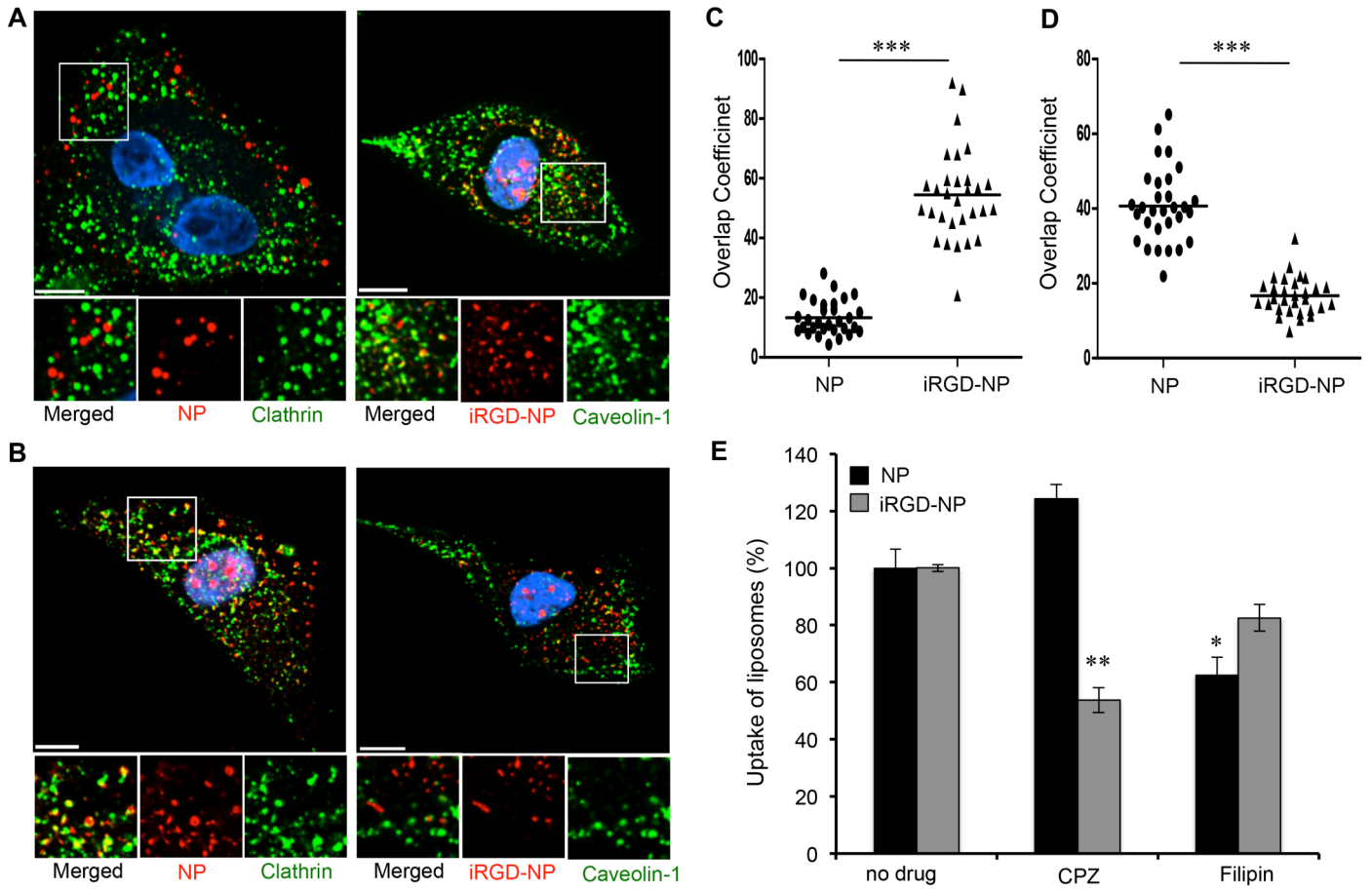

Figure 4: Clathrin-mediated internalization of iRGD-NPs and caveolin-dependent endocytosis of NPs. (A, B) HeLa cells were incubated with DiD-labeled NP nanoparticles (red, A) or DiD-labeled iRGD-NPs particles (red, B) for 30 min at 4°C to synchronize internalization. The cells were then incubated at 37°C for 15 min, fixed, permeabilized, and immunostained with anti-clathrin (green) or anti-caveolin-1 antibody (green). The nucleus of cells was counterstained with DAPI. Scale bar represents 10 μm. (C, D) Quantification of NP and iRGD-NP particles colocalized with clathrin (C) or caveolin-1 signals (D) after 15 min of incubation. Overlap coefficients were calculated using Manders' overlap coefficients by viewing more than 30 cells of each sample using the Nikon NIS-Elements software. Error bars represent the standard deviation of the mean from analysis of multiple images (***: $P < 0.005$). (E) Inhibition of clathrin-dependent endocytosis by chlorpromazine (CPZ, 25 μg/ml) and caveolin-dependent internalization by Filipin (10 μg/ml). The uptake of DiD-labeled NP and DiD-labeled iRGD-NP nanoparticles was determined by measuring DiD fluorescence via flow cytometry. Error bars represent the standard deviation of the mean from triplicate experiments (* $P < 0.05$, ** $P < 0.01$).

endosomes and further travel to lysosomes for possible release of drug from liposomes and endocytic compartments to cytosol. When taken together, the results showed that iRGD-NPs enter tumor cells via clathrin-dependent and receptor-mediated endocytosis, followed by transport through early endosomes and lysosomes.

Nanocapsules with LHRH peptide as targeting ligand After the successful development of clickable nanocapsules, we then tested methods to conjugate cancer-targeting ligands. We first selected the luteinizing hormone releasing hormone (LHRH) peptide 5 (Figure 5a), which binds to LHRH receptors that are overexpressed in various hormonal related cancers, such as breast and prostate cancers (Nagy and Schally, 2005). LHRH receptors are not expressed detectably in most visceral organs and have been targeted in the delivery of small molecules (Dharap et al., 2003; Dharap et al., 2005). The bifunctional dibenzocyclooctyne-PEG4-N-hydroxysuccinimidyl ester (DBCO-PEG4-NHS ester, 6, Figure 5a) was chosen as the tether. The peptide 5 was first conjugated to the NHS terminus of 6 through the internal D-Lys designed to serve as a site for coupling. The adduct 7 was verified by LC-MS and purified by HPLC to homogeneity. Subsequently, 7 was added to the azido-functionalized GFP nanocapsules at a molar ratio of 15:1 and allowed to react overnight at 4 °C. Following the click reaction, unreacted 7 was removed through ultrafiltration and the nanocapsules were dialyzed into PBS. To test the LHRH receptor mediated endocytosis of nanocapsules, we added the LHRH functionalized nanocapsules to MDA-MB-231 cells, which is known to overexpress the receptor (Harris et al., 1991). As controls, we also added GFP nanocapsules that are i) positively charged and are expected to be internalized; ii) azido-functionalized but not conjugated to LHRH; and iii) do not contain azido groups. After overnight incubation, the internalization of nanocapsules was visualized by fluorescence microscopy. As can be seen from Figure 5c, the positively charged nanocapsules were well-internalized as expected. In contrast, the neutral nanocapsules, either with or without azido groups, were not internalized into cell at all. LHRH-functionalized GFP nanocapsules, however, were efficiently internalized as can be seen from the GFP fluorescence in the cytoplasm. To quantify the extent of internalization through LHRH receptor, flow cytometry measurement was performed on samples. The level of internalization through LHRH receptor-mediated endocytosis is ~70% of that observed with positively charged nanocapsules. More importantly, azido-functionalized nanocapsules with LHRH-conjugation did not exhibit noticeable internalization compared to no

treatment or native GFP controls. Trafficking experiments were performed for the LHRH-targeted GFP nanocapsules. Localization in the early endosomes was observed within 30 minutes, while release into the cytoplasm was detected at one and two hours after delivery. No significant localization of GFP in the late endosome was observed.

To further test the selectivity of the protein delivery, we added the LHRH-functionalized nanocapsules to several cell lines with varying expression levels of LHRH receptor. When added to cervical cancer cell line HeLa cells that have comparable levels of expression, the amount of internalization were similar to that of MDA-MB-231 (Figure 5b). No internalization was seen with the SK-OV-3, which is a LHRH receptor-negative ovarian cancer cell line (Figure 5g). We then examined the targeting and internalization of the LHRH-targeted GFP nanocapsules after exposing them in FBS containing DMEM media at 37 °C for 24 and 49 hrs. No attenuation in internalization was observed compared to untreated nanocapsules, suggesting the targeting mechanism remained intact and the nanocapsules were stable under serum-like conditions.

Cytotoxicity of LHRH-conjugated p53 nanocapsules To examine the effect of delivered p53 on cell viability, we performed cytotoxicity studies using the LHRH-functionalized nanocapsules. Two different versions of p53 were used, the wild type and the tumor selective "super" p53 variant. The super p53 has the gain of function point mutant S121F that has been shown to display more potent apoptotic activity. The mutation alters the specificity of p53 in binding its targets, and in particular, attenuates the activation of MDM2 transcription associated with normal p53 overexpression. The decreased MDM2 feedback control therefore increases apoptosis induction. The S121F mutant kills tumor cells irrespective of p53 status but not wild-type

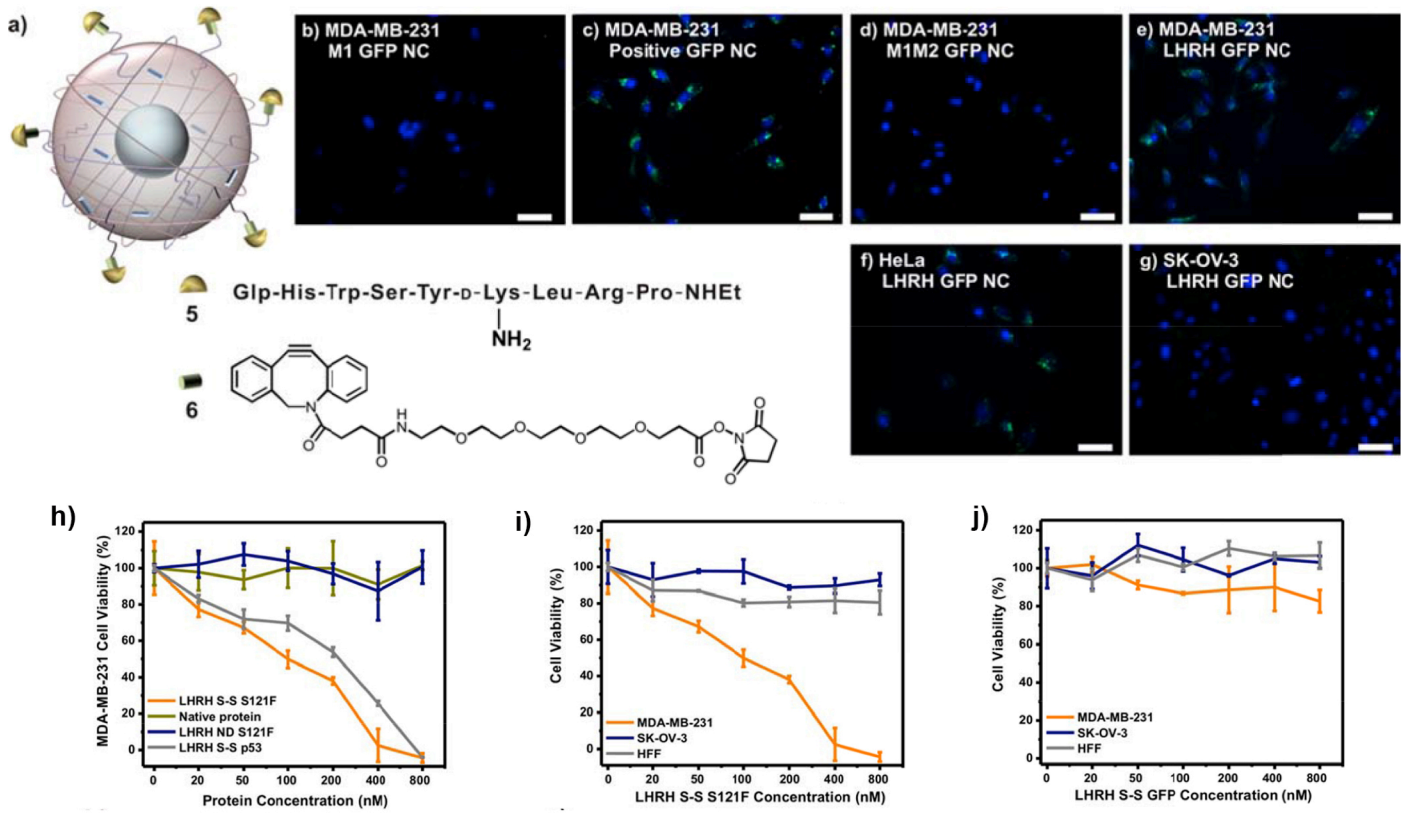

Figure 5: (a) Scheme of LHRH S-S nanocapsule. Glp is cyclized glutamine; (b-g) Fluorescence microscopy images of cell lines treated with 400 nM GFP-containing nanocapsules. b) MDA-MB-231 treated with GFP nanocapsules synthesized from monomer alone; (c) MDA-MB-231 treated with positively charged GFP nanocapsules; (d) MDA-MB-231 treated with GFP nanocapsules synthesized from monomers (no targeting ligand); (e) MDA-MB-231 treated with GFP nanocapsules synthesized from monomers and conjugated with LHRH peptide; (f) HeLa cells treated with nanocapsules in e; g) SK-OV-3 cells treated with nanocapsules in e. (h-j) Cytotoxicity of LHRH-conjugated nanocapsules towards cancer cell lines.

mouse embryo fibroblasts. S-S S121F NCs were prepared in the same manner as S-S p53 NC and conjugated to LHRH peptides using the click chemistry. Physical characterization was performed to verify that the nanocapsules were nearly identical in properties. Both LHRH-conjugated nanocapsules were then added to different cancer cell lines and the cytotoxicity was measured using MTS assay after 48 hrs. As shown in Figures 5h-5j, LHRH-conjugated S-S p53 NCs showed high selectivity towards MDA-MB-231 cells that overexpress the LHRH receptor. Nearly no toxicity was observed towards either SK-OV-3 or HFF at 800 nM, the highest concentration assayed. The S121F containing nanocapsules showed potent cytotoxicity, with IC50 at ~100 nM. In contrast, IC50 for the wild type p53 nanocapsules was ~300 nM. We confirmed observed cell death after delivery of S121F is indeed via apoptosis by using TUNEL assay. Negative controls were performed to ensure the observed toxicity is due to the combination of targeted delivery of p53 or tumor selective variant, including i) azido-functionalized S-S S121F NCs not conjugated to LHRH; ii) LHRH conjugated S-S GFP NCs; and iii) azido-functionalized GFP NCs not conjugated to LHRH. In all these controls, the cells remained unaffected by the addition of nanocapsules. These results therefore unequivocally confirm the targeted and functional delivery of p53 can be achieved using the encapsulation and conjugation strategies.

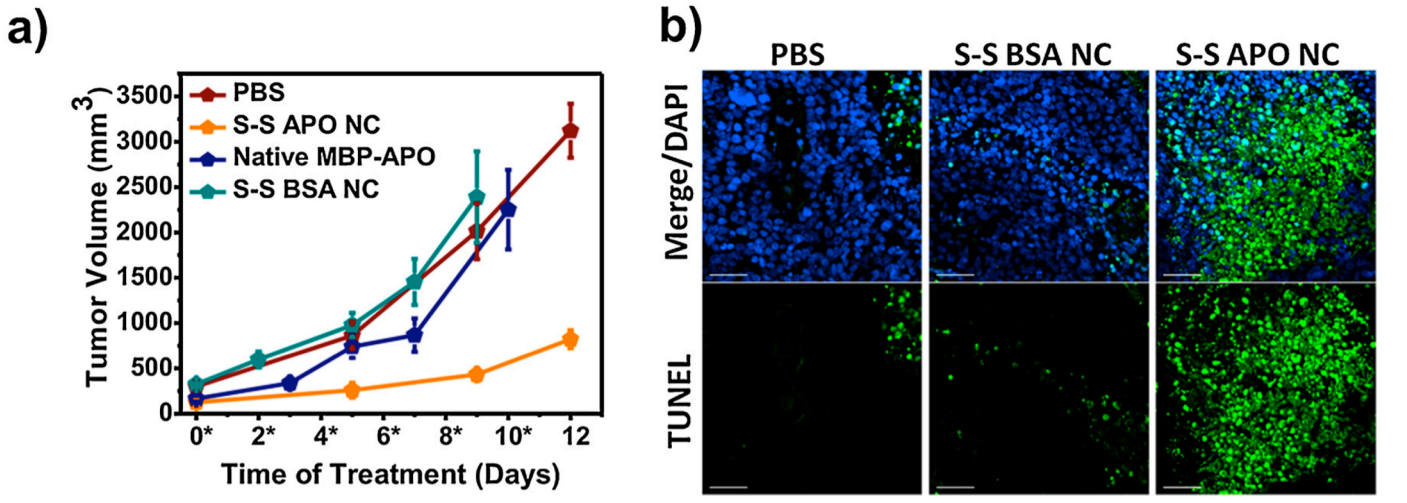

Figure 6: Treatment of apoptin nanocapsules resulted in tumor growth retardation. (a) Significant tumor inhibition was observed in mice treated by S-S APO NC. (b) Detection of apotosis in tumor tissues after treatment with different NCs.

Specific Aim 3: Examining the In Vivo Potency and Pharmacokinetics of the Nanocapsules

In vivo potency of apoptin nanocapsules We further examined the potency of S-S APO NC in a mouse xenograft model. Female athymic nude (nu/nu) mice were subcutaneously grafted on the back flank with $5x10^6$ MCF-7 breast cancer cells. When the tumor volume reached 100-200mm3 (day 0), mice were randomly separated into different groups and treated with intratumoral injection of PBS, MBP-APO, S-S APO NC. In addition, S-S NC with bovine serum albumin (S-S BSA NC) was added as a nonlethal protein cargo control to test the effects of the S-S NC polymer component on tumor cells in vivo. Tumors treated with saline, S-S BSA NC or native MBP-APO expanded rapidly and reached the maximum limit (> $2500mm^3$) within 12 days. In sharp contrast, tumor growth was significantly delayed when treated with S-S APO NC (Figure 6a). Fixed tumor tissues collected from each treatment group were examined for DNA fragmentation using in situ TUNEL assay. The images revealed the highest level of cell apoptosis for the tumor harvested from mice treated with S-S APO NC, correlating well with the significantly delayed tumor growth observed for this treatment group and confirming that tumor growth inhibition was indeed due to apoptin-mediated apoptosis (Figure 6b). Collectively, the xenograft study verified that the degradable NCs effectively delivered MBP-APO proteins to tumor cells in vivo, which was highly effective in limiting tumor progression. Upon further optimization of the pharmacokinetics of the S-S APO NC, these particles may be intravenously administered as an anticancer

therapy.

Pharmacokinetics and Biodistribution of Nanoparticles by PET Imaging For these tasks, we report our progress on utilizing positron emission tomography (PET) imaging to study in vivo biodistribution and pharmacokinetics of nanoparticles. We will still use the liposomal nanoparticles as the model system for testing the assays. For radiolabeling nanoparticles, amine-terminated PEG-SH was used for PEGylation of nanoparticles (UL and CML; UL: unilamellar nanoparticle; CML: crosslinked multilamellar nanoparticle), while DSPE-PEG-NH_2 was used for PEGylation of DLLs (Doxil-like nanoparticle), in order to introduce amine groups onto liposomes for further reaction (Figure 7a). ^{64}Cu was produced using the $^{64}Ni(p,n)^{64}Cu$ nuclear reaction and supplied in high specific activity as $^{64}CuCl_2$ in 0.1 N HCl. The bifunctional chelator AmBaSar was synthesized as reported (Cai et al., 2010). AmBaSar was activated by EDC and SNHS. Typically, 5 mg of AmBaSar (11.1 μmol) in 100 μL water and 1.9 mg of EDC (10 μmol) in 100 μL water were mixed together, and 0.1 N NaOH (150 μL) was added to adjust the pH to 4.0. SNHS (1.9 mg, 8.8 μmol) was then added to the stirring mixture on ice-bath, and 0.1 N NaOH was added to finalize the pH to 4.0. The reaction remained at 4 °C for 30 min. The theoretical concentration of active ester AmBaSar-OSSu was calculated to be 8.8 μmol. Then, 5–20 times AmBaSar-OSSu (based on molar ratios) were loaded to the liposomes of interest. The pH was adjusted to 8.5 using borate buffer (1M, pH 8.5). The reaction remained at 4 °C overnight, after which the size-exclusion PD-10 column was employed to afford the AmBaSar-conjugated liposomes in PBS buffer. AmBaSar-liposome was labeled with ^{64}Cu by addition of 1–5 mCi of ^{64}Cu (50–100 μg AmBaSar-liposome per mCi ^{64}Cu) in 0.1 N phosphate buffer (pH 7.5), followed by 45 min incubation at 40 °C. ^{64}Cu-AmBaSar-liposome was purified on a size exclusion PD-10 column using PBS as the elution solvent. Positron emission tomography (PET) imaging of the mice was performed using a microPET R4 rodent model scanner. The B16-F10 tumor-bearing C57/BL6 mice were imaged in the prone position in the microPET scanner. The mice were injected with approximately 100 μCi ^{64}Cu-AmBaSar-liposome via the tail vein. For imaging, the mice were anaesthetized with 2% isoflurane and placed near the center of the field of view (FOV), where the highest resolution and sensitivity are obtained. Static scans were obtained at 1, 3, and 24h post-injection. The images were reconstructed by a two-dimensional ordered subsets expectation maximum (2D-OSEM) algorithm. Time activity curves (TAC) of selected tissues were obtained by drawing regions of interest (ROI) over the tissue area. The counts per pixel/min obtained from the ROI were converted to counts per ml/min by using a calibration constant obtained from scanning a cylinder phantom in the microPET scanner. The ROI counts per ml/min were converted to counts per g/min, assuming a tissue density of 1 g/ml, and divided by the injected dose to obtain an image based on ROI-derived percent injected dose of ^{64}Cu tracer retained per gram (%ID/g). For biodistribution, animals were sacrificed 24h post-injection; tissues and organs of interest were harvested and weighed. Radioactivity in each organ was measured using a gamma counter, and radioactivity uptake was expressed as percent injected dose per gram (%ID/g). Mean uptake (%ID/g) for each group of animals was calculated.

As shown in Figure 7b, the PET images were obtained at several time points (1, 3, 24 h) after intravenous injection of ^{64}Cu-AmBaSar-labeled ULs, DLLs, or CMLs. After 1 h of administration, radioactivity was present mainly in well-perfused organs, and accumulation in tumors was detected in DLLs and CMLs compared with ULs. Furthermore, the accumulation of DLLs and CMLs in tumors significantly increased after 3 and 24 h of injection, whereas accumulation of ULs in the bladder was observed after 3 h of administration as a consequence of rapid degradation. In addition, the tumors and tissues of interest were then excised at 24 h post-injection and weighed, and accumulation levels of particles in the tumors and tissues were determined by measuring radioactivity (Figure 7c). This biodistribution assay revealed significantly higher accumulation of CMLs in tumors than that of ULs with the same lipid composition, suggesting that CMLs with improved vesicle stability could indeed enhance accumulation of drug carriers at the tumor site.

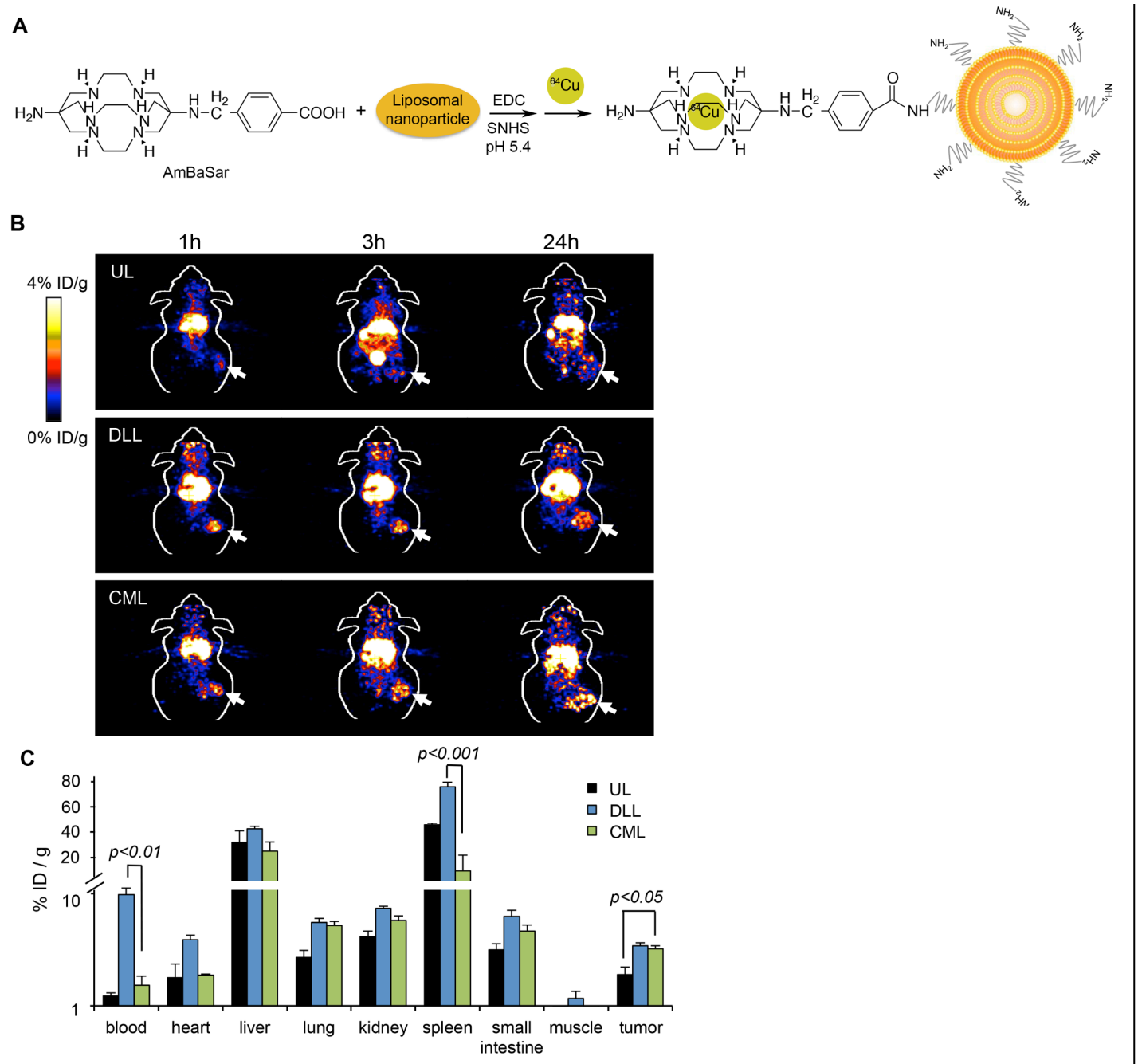

Figure 7: Biodistribution of drug carriers and accumulation of Dox in tumors. (a) Preparation of ^{64}Cu-AmBaSar-labeled liposomes. (b) *In vivo* PET images of C57/BL6 mice bearing B16 tumors at 1, 3, and 24 h post-injection of ^{64}Cu-AmBaSar-labeled UL, DLL, or CML. (c) Biodistribution of liposomes in different tissues at 24 h after injection with ^{64}Cu-AmBaSar-labeled UL, DLL, or CML shown as percentage of injection dose per g of tissues (% ID/g).

4. IMPACT

We are able to deliver most milestones promised in the original proposal. We also believe that the entire work described in this report has significant impact on cancer research and cancer treatment. Before this work, this was no single method of intracellular protein delivery that could be used to deliver functional proteins into cells. As a result, while many proteins had been found to have potent and specific antitumor properties, there was no general method of administering them as part of anticancer therapy. However, upon completion of this project, we have demonstrated a general method of protein-based chemotherapy. Our work opens potential clinical routes to administer protein

drugs to breast cancer patients, without using the gene therapy approaches. Two target proteins, apoptin and p53, have been demonstrated to be effective to induce rapid apoptosis in breast tumor cells in vitro and in vivo, offering supporting evidence for further translational studies in clinic settings. Our targeting studies using iRGD and LHRH peptides conclude that they are promising targeting reagents that can be introduced to nanocapsules to further enhance breast cancer therapy. Therefore, we firmly believe the impact of our nanocapsule work is high and this innovative approach can help cure breast cancer.

5. REFERENCES

Atkins, J.H., and Gershell, L.J. (2002). Selective anticancer drugs. Nature reviews Drug discovery *1*, 491-492.
Backendorf, C., Visser, A.E., de Boer, A.G., Zimmerman, R., Visser, M., Voskamp, P., Zhang, Y.H., and Noteborn, M. (2008). Apoptin: therapeutic potential of an early sensor of carcinogenic transformation. Annual review of pharmacology and toxicology *48*, 143-169.

Bareford, L.M., and Swaan, P.W. (2007). Endocytic mechanisms for targeted drug delivery. Adv Drug Deliv Rev *59*, 748-758.

Blagosklonny, M.V. (2002). Oncogenic resistance to growth-limiting conditions. Nature reviews Cancer *2*, 221-225.

Brown, C.J., Lain, S., Verma, C.S., Fersht, A.R., and Lane, D.P. (2009). Awakening guardian angels: drugging the p53 pathway. Nature reviews Cancer *9*, 862-873.

Cai, H., Li, Z., Huang, C.W., Park, R., Shahinian, A.H., and Conti, P.S. (2010). An improved synthesis and biological evaluation of a new cage-like bifunctional chelator, 4-((8-amino-3,6,10,13,16,19-hexaazabicyclo[6.6.6]icosane-1-ylamino)methyl) benzoic acid, for 64Cu radiopharmaceuticals. Nucl Med Biol *37*, 57-65.

Carlsson, S.R., Roth, J., Piller, F., and Fukuda, M. (1988). Isolation and Characterization of Human Lysosomal Membrane-Glycoproteins, H-Lamp-1 and H-Lamp-2 - Major Sialoglycoproteins Carrying Polylactosaminoglycan. J Biol Chem *263*, 18911-18919.

Cho, M.H., Lee, E.J., Son, M., Lee, J.H., Yoo, D., Kim, J.W., Park, S.W., Shin, J.S., and Cheon, J. (2012). A magnetic switch for the control of cell death signalling in in vitro and in vivo systems. Nature materials *11*, 1038-1043.

Chorny, M., Hood, E., Levy, R.J., and Muzykantov, V.R. (2010). Endothelial delivery of antioxidant enzymes loaded into non-polymeric magnetic nanoparticles. Journal of controlled release : official journal of the Controlled Release Society *146*, 144-151.

Christoforidis, S., McBride, H.M., Burgoyne, R.D., and Zerial, M. (1999). The Rab5 Effector Eea1 is a Core Component of Endosome Docking. Nature *397*, 621-625.

Coles, C., Condie, A., Chetty, U., Steel, C.M., Evans, H.J., and Prosser, J. (1992). p53 mutations in breast cancer. Cancer research *52*, 5291-5298.

Conner, S.D., and Schmid, S.L. (2003). Regulated portals of entry into the cell. Nature, 37-44.

Cotter, T.G. (2009). Apoptosis and cancer: the genesis of a research field. Nature reviews Cancer *9*, 501-507.
Danen-Van Oorschot, A.A., Fischer, D.F., Grimbergen, J.M., Klein, B., Zhuang, S., Falkenburg, J.H., Backendorf, C., Quax, P.H., Van der Eb, A.J., and Noteborn, M.H. (1997). Apoptin induces apoptosis in human

transformed and malignant cells but not in normal cells. Proceedings of the National Academy of Sciences of the United States of America *94*, 5843-5847.

Danen-Van Oorschot, A.A., Zhang, Y.H., Leliveld, S.R., Rohn, J.L., Seelen, M.C., Bolk, M.W., Van Zon, A., Erkeland, S.J., Abrahams, J.P., Mumberg, D*., et al.* (2003). Importance of nuclear localization of apoptin for tumor-specific induction of apoptosis. The Journal of biological chemistry *278*, 27729-27736.

Dharap, S.S., Qiu, B., Williams, G.C., Sinko, P., Stein, S., and Minko, T. (2003). Molecular targeting of drug delivery systems to ovarian cancer by BH3 and LHRH peptides. Journal of controlled release : official journal of the Controlled Release Society *91*, 61-73.

Dharap, S.S., Wang, Y., Chandna, P., Khandare, J.J., Qiu, B., Gunaseelan, S., Sinko, P.J., Stein, S., Farmanfarmaian, A., and Minko, T. (2005). Tumor-specific targeting of an anticancer drug delivery system by LHRH peptide. Proceedings of the National Academy of Sciences of the United States of America *102*, 12962-12967.

Dobson, P.D., and Kell, D.B. (2008). Carrier-mediated Cellular Uptake of Pharmaceutical Drugs: an Exception or the Rule? Nat Rev Drug Discov *7*, 205-220.

Evan, G.I., and Vousden, K.H. (2001). Proliferation, cell cycle and apoptosis in cancer. Nature *411*, 342-348.

Feron, O. (2010). Tumor-penetrating peptides: a shift from magic bullets to magic guns. Sci Transl Med *2*.

Friedler, A., Hansson, L.O., Veprintsev, D.B., Freund, S.M., Rippin, T.M., Nikolova, P.V., Proctor, M.R., Rudiger, S., and Fersht, A.R. (2002). A peptide that binds and stabilizes p53 core domain: chaperone strategy for rescue of oncogenic mutants. Proceedings of the National Academy of Sciences of the United States of America *99*, 937-942.

Giannotti, M.I., Esteban, O., Oliva, M., Garcia-Parajo, M.F., and Sanz, F. (2011). pH-responsive polysaccharide-based polyelectrolyte complexes as nanocarriers for lysosomal delivery of therapeutic proteins. Biomacromolecules *12*, 2524-2533.

Gibbs, J.B. (2000). Mechanism-based target identification and drug discovery in cancer research. Science *287*, 1969-1973.

Gu, Z., Biswas, A., Zhao, M., and Tang, Y. (2011). Tailoring nanocarriers for intracellular protein delivery. Chemical Society reviews *40*, 3638-3655.

Guelen, L., Paterson, H., Gaken, J., Meyers, M., Farzaneh, F., and Tavassoli, M. (2004). TAT-apoptin is efficiently delivered and induces apoptosis in cancer cells. Oncogene *23*, 1153-1165.

Harris, N., Dutlow, C., Eidne, K., Dong, K.W., Roberts, J., and Millar, R. (1991). Gonadotropin-releasing hormone gene expression in MDA-MB-231 and ZR-75-1 breast carcinoma cell lines. Cancer research *51*, 2577-2581.

Hu, Y., Atukorale, P.U., Lu, J.J., Moon, J.J., Um, S.H., Cho, E.C., Wang, Y., Chen, J., and Irvine, D.J. (2009). Cytosolic delivery mediated via electrostatic surface binding of protein, virus, or siRNA cargos to pH-responsive core-shell gel particles. Biomacromolecules *10*, 756-765.

Issaeva, N., Bozko, P., Enge, M., Protopopova, M., Verhoef, L.G., Masucci, M., Pramanik, A., and Selivanova, G. (2004). Small molecule RITA binds to p53, blocks p53-HDM-2 interaction and activates p53 function in tumors. Nature medicine *10*, 1321-1328.

Lacroix, M., Toillon, R.A., and Leclercq, G. (2006). p53 and breast cancer, an update. Endocrine-related cancer *13*, 293-325.

Le Roy, C., and Wrana, J.L. (2005). Clathrin- and Non-clathrin-mediated Endocytic Regulation of Cell Signalling. Nat Rev Mol Cell Biol *6*, 112-126.

Lee, Y., Ishii, T., Cabral, H., Kim, H.J., Seo, J.H., Nishiyama, N., Oshima, H., Osada, K., and Kataoka, K. (2009). Charge-conversional polyionic complex micelles-efficient nanocarriers for protein delivery into cytoplasm. Angewandte Chemie *48*, 5309-5312.

Leliveld, S.R., Zhang, Y.H., Rohn, J.L., Noteborn, M.H., and Abrahams, J.P. (2003). Apoptin induces tumor-specific apoptosis as a globular multimer. The Journal of biological chemistry *278*, 9042-9051.

Liechty, W.B., Chen, R., Farzaneh, F., Tavassoli, M., and Slater, N.K. (2009). Synthetic pH-Responsive Polymers for Protein Transduction. Advanced materials *21*, 3910-3914.

Luzio, J.P., Brake, B., Banting, G., Howell, K.E., Braghetta, P., and Stanley, K.K. (1990). Identification, Sequencing and Expression of an Integral Membrane-Protein of the Trans-Golgi Network (Tgn38). Biochem J *270*, 97-102.

Mitra, A., Mulhollan, J., Nan, A., McNeillb, E., Ghandehari, H., and Line, B.R. (2005). Targeting tumor angiogenic vasculature using polymer–RGD conjugates. J Control Release *102*, 191-201.

Murphy, E.A., Majeti, B.K., Barnes, L.A., Makale, M., Weis, S.M., Lutu-Fuga, K., Wrasidlo, W., and Cheresh, D.A. (2008). Nanoparticle-mediated drug delivery to tumor vasculature suppresses metastasis. Proc Natl Acad Sci USA *105*, 9343-9348.

Nagy, A., and Schally, A.V. (2005). Targeting cytotoxic conjugates of somatostatin, luteinizing hormone-releasing hormone and bombesin to cancers expressing their receptors: a "smarter" chemotherapy. Current pharmaceutical design *11*, 1167-1180.

Neufeld, E.B., Cooney, A.M., Pitha, J., Dawidowicz, E.A., Dwyer, N.K., Pentchev, P.G., and BlanchetteMackie, E.J. (1996). Intracellular Trafficking of Cholesterol Monitored with a Cyclodextrin. J Biol Chem *271*, 21604-21613.

Pelkmans, L., and Helenius, A. (2002). Endocytosis Via Caveolae. Traffic *3*, 311-320.

Pelkmans, L., Kartenbeck, J., and Helenius, A. (2001). Caveolar Endocytosis of Simian Virus 40 Reveals a New Two-step Vesicular-transport Pathway to the ER. Nat Cell Biol *3*, 473-483.

Petros, R.A., and DeSimone, J.M. (2010). Strategies in the Design of Nanoparticles for Therapeutic Applications. Nat Rev Drug Discov *9*, 615-627.

Reed, J.C. (2003). Apoptosis-targeted therapies for cancer. Cancer cell *3*, 17-22.

Rothberg, K.G., Heuser, J.E., Donzell, W.C., Ying, Y.S., Glenney, J.R., and Anderson, R.G.W. (1992). Caveolin, a Protein-Component of Caveolae Membrane Coats. Cell *68*, 673-682.

Senzer, N., Nemunaitis, J., Nemunaitis, M., Lamont, J., Gore, M., Gabra, H., Eeles, R., Sodha, N., Lynch, F.J., Zumstein, L.A*., et al.* (2007). p53 therapy in a patient with Li-Fraumeni syndrome. Molecular cancer therapeutics *6*, 1478-1482.

Sugahara, K.N., Teesalu, T., Karmali, P.P., Kotamraju, V.R., Agemy, L., Girard, O.M., Hanahan, D., Mattrey, R.F., and Ruoslahti, E. (2009). Tissue-penetrating delivery of compounds and nanoparticles into tumors. Cancer Cell *16*, 510-520.

Vassilev, L.T., Vu, B.T., Graves, B., Carvajal, D., Podlaski, F., Filipovic, Z., Kong, N., Kammlott, U., Lukacs, C., Klein, C.*, et al.* (2004). In vivo activation of the p53 pathway by small-molecule antagonists of MDM2. Science *303*, 844-848.

Wang, L.H., Rothberg, K.G., and Anderson, R.G.W. (1993). Mis-Assembly of Clathrin Lattices on Endosomes Reveals a Regulatory Switch for Coated Pit Formation. J Cell Biol *123*, 1107-1117.

Zhao, M., Biswas, A., Hu, B., Joo, K.I., Wang, P., Gu, Z., and Tang, Y. (2011). Redox-responsive nanocapsules for intracellular protein delivery. Biomaterials *32*, 5223-5230.

Zhuang, S.M., Shvarts, A., van Ormondt, H., Jochemsen, A.G., van der Eb, A.J., and Noteborn, M.H. (1995). Apoptin, a protein derived from chicken anemia virus, induces p53-independent apoptosis in human osteosarcoma cells. Cancer research *55*, 486-489.

6. CHANCES/PROBLEMS

N/A

7. PRODUCTS

Zhao, M., Hu, B., Gu, Z., Joo, K., Wang, P., Tang, Y. "Degradable Polymeric Nanocapsule for Efficient Intracellular Delivery of a High Molecular Weight Tumor-Selective Protein Complex." *Nano Today.* **2013**, 8, 11-20.

Zhao, M., Liu, Y., Hsieh, R.S., Wang, N., Tai, W., Joo, J.I., Wang, P., Gu, Z., Tang, Y., "Clickable Protein Nanocapsules for Targeted Delivery of Recombinant p53 Protein", J. Am. Chem. Soc., **2014**, in revision.

8. PARTICIPANTS & OTHER COLLABORATING ORGANIZATIONS

Participants

Name: Bingbing Dai
Project Role: Graduate Student
Months Worked: 2
Contribution to Project: Performed animal work

Name: Jinxu Fang
Project Role: Graduate Student
Months Worked: 9
Contribution to Project: Performed cell culture and animal work

Name: Xiaolu Han
Project Role: Graduate Student
Months Worked: 5
Contribution to Project: Performed cell culture work

Name: Biliang Hu
Project Role: Graduate Student
Months Worked: 6
Contribution to Project: Performed in vivo animal work

Name: Yarong Liu

Project Role: Graduate Student
Months Worked: 5
Contribution to Project: Performed the internalization study

Name: Liang Xiao
Project Role: Graduate Student
Months Worked: 4
Contribution to Project: Performed the biodistribution study

Name: Chupei Zhang
Project Role: Graduate Student
Months Worked: 6
Contribution to Project: Performed cell culture and animal work

Name: Pin Wang
Project Role: Principal Investigator
Months Worked: 36
Contribution to Project: Supervised the overall project
Funding Support: NIH

Collaborating Organizations

University of California Los Angels

9. SPECIAL REPORTING REQUIREMENTS

N/A

10. APPENDICES

Nano Today (2013) 8, 11—20

Available online at www.sciencedirect.com

SciVerse ScienceDirect

journal homepage: www.elsevier.com/locate/nanotoday

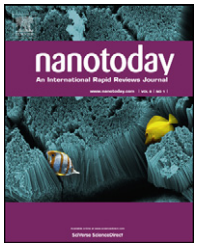

RAPID COMMUNICATION

Degradable polymeric nanocapsule for efficient intracellular delivery of a high molecular weight tumor-selective protein complex

Muxun Zhao[a], Biliang Hu[b], Zhen Gu[a,1], Kye-Il Joo[b], Pin Wang[b,], Yi Tang[a,c,*]**

[a] *Department of Chemical and Biomolecular Engineering, University of California, Los Angeles, CA 90095, USA*
[b] *Mork Family Department of Chemical Engineering and Materials Science, University of Southern California, Los Angeles, CA 90089, USA*
[c] *California NanoSystems Institute, University of California, Los Angeles, CA 90095, USA*

Received 29 May 2012; received in revised form 4 November 2012; accepted 26 December 2012
Available online 1 February 2013

KEYWORDS
Nanogel;
Core—shell;
Redox-responsive;
Apoptosis;
Breast cancer

Summary The development of stimuli-responsive, nano-scale therapeutics that selectively target and attack tumors is a major research focus in cancer nanotechnology. A potent therapeutic option is to directly arming the cancer cells with apoptotic-inducing proteins that are not affected by tumoral anti-apoptotic maneuvers. The avian virus-derived apoptin forms a high-molecular weight protein complex that selectively accumulates in the nucleus of cancer cell to induce apoptotic cell death. To achieve the efficient intracellular delivery of this tumor-selective protein in functional form, we synthesized degradable, sub-100 nm, core—shell protein nanocapsules containing the 2.4 MDa apoptin complexes. Recombinant apoptin is reversibly encapsulated in a positively charged, water soluble polymer shell and is released in native form in response to reducing conditions such as the cytoplasm. As characterized by confocal microscopy, the nanocapsules are efficiently internalized by mammalian cells lines, with accumulation of rhodamine-labeled apoptin in the nuclei of cancer cells only. Intracellularly released apoptin induced tumor-specific apoptosis in several cancer cell lines and inhibited tumor growth *in vivo*, demonstrating the potential of this polymer—protein combination as an anticancer therapeutic.

Abbreviations: NC, nanocapsule; APO, apoptin; S—S, disulfide bonded; AAm, acrylamide; APMAAm, *N*-(3-aminopropyl)methacrylamide; MBP, maltose binding protein; Rho, rhodamine; ND, nondegradable; HFF, human foreskin fibroblast.

* Corresponding author at: 420 Westwood Plaza, Los Angeles, CA 90095, USA. Tel.: +1 310 825 0375; fax: +1 310 206 4107.
** Corresponding author at: 925 Bloom Walk, HED 216, Los Angeles, CA 90089, USA. Tel.: +1 213 740 0780; fax: +1 213 740 7223.
E-mail addresses: pinwang@usc.edu (P. Wang), yitang@ucla.edu (Y. Tang).
[1] Current address: Joint Department of Biomedical Engineering, University of North Carolina at Chapel Hill, North Carolina State University, Raleigh, NC 27606, USA.

1748-0132/$ — see front matter © 2013 Elsevier Ltd. All rights reserved.
http://dx.doi.org/10.1016/j.nantod.2012.12.003

Introduction

The most desirable anticancer therapy is both potent and specific toward tumor cells [1,2]. Many conventional small molecule chemotherapeutics do not discriminate between cancerous and normal cells, cause damage to healthy tissues, and are therefore unable to be administered at high dosage. In contrast, cytoplasmic and nuclear proteins that selectively alter the signaling pathways in tumor cells, reactivate apoptosis and restore tissue homeostasis, can delay tumor progression with less collateral damage to other tissues [3—6]. Using stimuli-responsive nanocarriers for the intracellular delivery of such proteins, including human tumor suppressors [7] and exogenous tumor-killing proteins [8—10]), is attractive as a new anti-cancer therapy modality.

Apoptin is a 121-residue protein derived from chicken anemia virus [9]. When transgenically expressed, apoptin can induce p53-independent apoptosis in a variety of tumor and transformed cells [11,12], while leaving normal and untransformed cells unaffected [13]. Apoptin exists as a globular multimeric complex, composed of thirty to forty subunits, with no well-defined secondary structure [14]. While the exact mechanism of the tumor selectivity is unresolved, apoptin is known to translocate to the nucleus where tumor-specific phosphorylation at residue Thr108 takes place, leading to accumulation of apoptin in nucleus and activation of the apoptotic cascade in tumor cell [15]. In normal cells, apoptin is not phosphorylated at Thr108 and is located mostly in the cytoplasm, where it aggregates and undergoes degradation [16]. Because of the high potency in inducing this exquisite tumor-selective apoptosis, apoptin has been investigated widely as an anti-tumor therapeutic option [9]. Different gene therapy approaches have been used to administer apoptin to mouse xenograft tumor models, in which significant reduction in tumor sizes and prolonged lifespan of mice have been observed without compromising the overall health [17—19]. However, as with other gain-of-function therapy candidates, *in vivo* gene delivery approaches using viral vectors may lead to unwanted genetic modifications and elicit safety concerns [20]. While protein transduction domain (PTD)-fused apoptin has been delivered to cells [21,22], this approach suffers from inefficient release of the cargo from endosomes and instability of the unprotected protein [23]. Development of nanoparticle carriers to aid the functional delivery of apoptin to tumor cells is therefore desirable [24].

We chose to work with recombinant maltose-binding-protein fused apoptin (MBP—APO) that can be solubly expressed from *Escherichia coli*, whereas native apoptin forms inclusion bodies [14]. MBP—APO has been shown to similarly assemble into a multimeric protein complex, which exhibits the essential functions and selectivity of native apoptin [14]. Nanoparticle-mediated delivery of functional MBP—APO poses unique challenges [25]. First, MBP—APO preassembles into large complex with an average diameter of ~40 nm and molecular weight of ~2.4 MDa [14]. To achieve nanocarrier sizes that are optimal for *in vivo* administration (~100 nm) [26], a loading strategy that forms compact particles is desirable. Second, in order to maintain the multimeric state of functional MBP—APO, the protein loading and releasing steps need to take place under very mild, physiological conditions in the absence of surfactants. Lastly, the nanocarrier must completely disassemble inside the cell to release the MBP—APO in its native and unobstructed form to ensure the correct spatial presentation of key residues within the apoptin portion, including the nuclear localization/export signals, the phosphorylation site and other elements important for downstream signaling.

In the current study, we selected a polymeric nanocapsule (NC) strategy for the functional delivery of MBP—APO, in which the protein complex is noncovalently protected in a water soluble polymer shell (Fig. 1). This slightly positively charged shell shields the MBP—APO from serum proteases and surrounding environment, while enabling cellular uptake of the polymer—protein complex through endocytosis [27]. The polymeric layer is weaved together by redox-responsive cross-linkers containing disulfide bond (S—S) that can be degraded once the NCs are exposed to the reducing environment in cytoplasm [28]. No covalent bonds are formed between the protein cargo and the polymer shell, which ensures complete disassembly of the capsule layer and release of native MBP—APO inside the cell. Using this approach, we show that MBP—APO can be efficiently delivered to induce apoptosis in cancer cell lines selectively both *in vitro* and *in vivo*.

Materials and methods

Materials

N-(3-aminopropyl)methacrylamide hydrochloride was purchased from Polymer Science, Inc. CellTiter 96® AQueous One Solution Cell Proliferation Assay (MTS) reagent was purchased from Promega Corporation. APO-BrdU™ TUNEL Assay Kit was purchased from Invitrogen. *In Situ* Cell Death Detection Kit, POD; was purchased from Roche Applied Science. Female athymic nude (*nu*/*nu*) mice, 6 weeks of age, were purchased from Charles River Laboratories (Wilmington, MA). All other chemicals were purchased from Sigma—Aldrich and used as received.

Protein nanocapsule preparation

The concentration of protein was diluted to 1 mg/mL with 5 mM sodium bicarbonate buffer at pH 9. Then 200 mg/mL acrylamide (AAm) monomer was added to 1 mL of protein solution with stirring at 4 °C. After 10 min, the second monomer, *N*-(3-aminopropyl)methacrylamide (APMAAm), was added while stirring. Different cross-linkers, *N*,*N*′-methylene bisacrylamide for ND NC and *N*,*N*′-bis(acryloyl)cystamine for S—S NC, were added 5 min after the addition of APMAAm. The polymerization reaction was immediately initiated by adding 30 μL of ammonium persulfate (100 mg/mL, dissolved in deoxygenated and deionized water) and 3 μL of *N*,*N*,*N*′,*N*′-tetramethylethylenediamine. The polymerization reaction was allowed to proceed for 60 min. The molar ratios of AAm/APMAAm/cross-linker used were

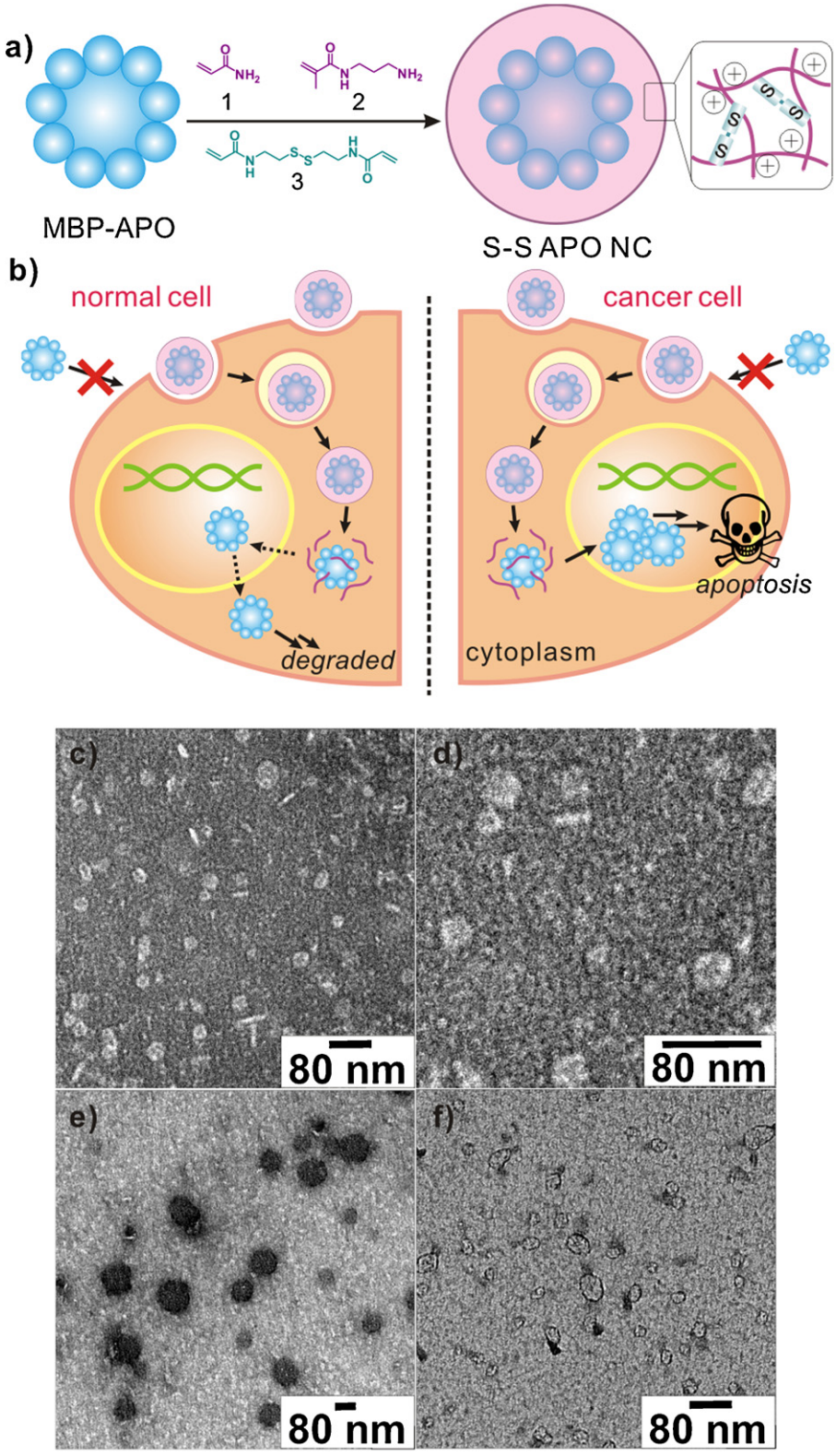

Figure 1 Degradable nanocapsules for apoptin delivery. (a and b) Schematic diagram of synthesis of degradable apoptin nanocapsules (S—S APO NC) and delivery into tumor cells to induce apoptosis; TEM images of (c) native MBP—APO; (d) enlarged image of MBP—APO; (e) S—S APO NC; and (f) degraded S—S APO NC after treatment with 2 mM GSH for 6 h at 37 °C.

1.5:1:0.14, 2:1:0.14, 4:1:0.14, and 8:1:0.14. Buffer exchange with phosphate-buffered saline (PBS) buffer (pH 7.4) was used to remove the remaining monomers and initiators. Rhodamine-labeled APO NCs was obtained through encapsulation of MBP—APO modified with 5-carboxy-X-rhodamine *N*-succinimidyl ester (mass ratio (MBP—APO:rhodamine) = 4:1).

Characterization of protein nanocapsules

The mean hydrodynamic size and ζ-potential of NC were determined by dynamic light scattering (DLS) in PBS buffer. Samples of NCs (0.05 mg/mL) for TEM imaging were negatively stained with 2% uranyl acetate in alcoholic solution (50% ethanol). The lamella of stained sample was prepared on carbon-coated electron microscopy grids (Ted Pella, Inc.).

Cellular uptake and localization of nanocapsules

MDA-MB-231, HeLa, MCF-7, and human foreskin fibroblast (HFF) cells (ATCC, Manassas, VA) were cultured in Dulbecco's modified Eagle's media (DMEM) (Invitrogen) supplemented with 10% bovine growth serum (Hyclone, Logan, UT), 1.5 g/L sodium bicarbonate, 100 μg/mL streptomycin and 100 U/mL penicillin, at 37 °C with 98% humidity and 5% CO_2. To visualize NCs uptake, MDA-MB-231 cells were seeded into 48-well plate, with a density of 10,000 cells/well in 250 μL of media with supplements. S—S Rho—APO NC and ND Rho—APO NC were added to a final concentration of 20 nM. After 1 h and 24 h of incubation, cells were washed with PBS twice, stained with DAPI Nucleic Acid Stain and imaged. For internalization of S—S Rho—APO NC with different ζ-potentials, MDA-MB-231 cells were incubated with 20 nM NCs for 2 h before nuclei staining. Markers for early and late endosomes were used for internalization trafficking study. A concentration of 20 nM S—S Rho—APO NCs was added to HeLa cells and incubated for 30 min, 60 min and 120 min under 37 °C. Cells were then fixed with 4% formaldehyde, permeabilized with 0.1% Triton X-100, and stained with antibodies, mouse anti-EEA1 antibody against early endosomes and rabbit anti-CI-MPR antibody against late endosomes (Cell Signaling Technology, Inc.). Texas red goat anti-mouse IgG and Alexa Fluor® 647 goat anti-rabbit IgG (Invitrogen) were added as the secondary antibody. To determine the cellular localization of the protein delivered, confocal images were taken with HeLa, MCF-7, and HFF cells incubated with 20 nM of S—S Rho—APO NC or ND Rho—APO NC at 37 °C for 24 h. Nuclei were then counterstained with DAPI. The Z-stack images of cells were imaged at 0.4-μm intervals and analyzed by Nikon NIS Element software. Fluorescent microscopy images were acquired on a Yokogawa spinning-disk confocal scanner system (Solamere Technology Group, Salt Lake City, UT) using a Nikon eclipse Ti-E microscope equipped with a 60×/1.49 Apo TIRF oil objective and a Cascade II: 512 EMCCD camera (Photometrics, Tucson, AZ, USA). An AOTF (acousto-optical tunable filter) controlled laser-merge system (Solamere Technology Group Inc.) was used to provide illumination power at each of the following laser lines: 491 nm, 561 nm, and 640 nm solid state lasers (50 mW for each laser).

Cytotoxicity assays

Different cancer cells lines, HeLa, MCF-7 and MDA-MB-231, as well as noncancerous HFF, were seeded into 96-well plates, each well containing 5000 cells in 100 μL of DMEM with supplements. Different concentrations of protein and NCs were added into each well and the plates. After incubation of 48 h at 37 °C, the wells were washed with PBS solution twice and 100 μL of fresh cell culture media with supplements was added. Then 20 μL MTS solution (CellTiter 96® AQueous One Solution Cell Proliferation Assay) was added into each well and the plates were incubated for 3 h at 37 °C. The absorbance of each well was read at 490 nm using a microplate reader (PowerWave X, Bio-tek Instruments, USA). Apoptosis was detected using APO-BrdU Terminal Deoxynucleotidyl Transferase dUTP Nick End Labeling (TUNEL) assay kit. MDA-MB-231 and HFF cells were seeded at a density of 100,000 cells/well into a 6-well plate in 2 mL of cell culture media with supplements. Proteins and NCs were added after cells covered 80% of bottom surface. After 24 h of incubation, cells were fixed with 1% paraformaldehyde in PBS, followed by the addition of DNA labeling solution containing terminal deoxynucleotidyl transferase and bromodeoxyuridine (BrdUrd). Cells were then stained with Alexa Fluor® 488 dye-labeled anti-BrdUrd antibody. Samples were deposited onto slides, which were later stained with propidium iodide (PI) solution containing RNase A. Images were obtained by fluorescent microscope (Zeiss, Observer Z1) using appropriate filters for Alexa Fluor 488 and PI.

In vivo studies with MCF-7 xenograft model

All mice were housed in an animal facility at the University of Southern California in accordance with institute regulations. Female athymic nude (*nu*/*nu*) mice were subcutaneously grafted on the back flank with 5×10^6 MCF-7 tumor cells. Afterwards, tumor size was monitored by a fine caliper and the tumor volume was calculated as the product of the two largest perpendicular diameters and the vertical thickness ($L \times W \times D$, mm^3). When the tumor volume reached 100—200 mm^3, mice were randomly separated into different groups. From day 0, mice were treated with intratumoral injection of native MBP—APO or S—S APO NC (200 μg per mouse) every other day. PBS and S—S BSA NC were included as the negative controls. When the tumor volume exceeded 2500 mm^3, the mice were euthanized by CO_2 according animal protocol. The average of tumor volumes was plotted as the tumor growth curve in respective treated groups. For histology study, treated tumor samples were collected and fixed in 4% paraformaldehyde, and processed for staining using the *In Situ* Cell Death Detection Kit. The stained tumor slides were observed under microscope, and representative pictures were taken for analysis. Paraformaldehyde-postfixed frozen tumor sections (5-μm thick) were permeabilized with 0.1% triton X-100 and stained with TUNEL assay kit (*In Situ* Cell Death Detection Kit, POD; Roche Applied Science, Indianapolis, IN) in accordance with

the manufacturer's instructions. DAPI was used for nuclear counterstaining.

Results and discussion

Synthesis and characterization of apoptin nanocapsules

MBP—APO (p*I* = 6.5) was first purified from *E. coli* extract using an amylose-affinity column (Supplement 2 and Supplement 8). Dynamic light scattering (DLS) measurement revealed an average hydrodynamic radius of 36.1 nm (Supplement 3), consistent with the reported size for the recombinant MBP—APO complex [14]. Transmission electron microscopy (TEM) analysis of MBP—APO showed similarly sized protein complexes (Fig. 1c and enlarged in Fig 1d). Interestingly, MBP—APO complexes appear to adopt a disk-shaped structure despite the lack of defined secondary structure from the apoptin component. Since the apoptin portion of the protein can self-assemble into the ~40-mer complex, we propose a three dimensional arrangement of MBP—APO in which the C-terminal apoptin forms the central spoke of the wheel-like structure (Fig. 1a), with the larger MBP portion distributes around the apoptin. The planar arrangement allows the apoptin portion of the fusion protein to remain accessible to its protein partners, which may explain how the MBP—APO fusion retains essentially all of the observed functions of native apoptin.

The reversible encapsulation strategy for producing apoptin NCs is shown in Fig. 1a. Following electrostatic deposition of the monomers acrylamide (**1** in Fig. 1a) and *N*-(3-aminopropyl)methacrylamide (**2**), and the cross-linker *N*,*N*′-bis(acryloyl)cystamine (**3**), at a molar ratio of 1.5:1:0.14, onto MBP—APO (1 mg) in carbonate buffer (5 mM, pH 9.0), *in situ* polymerization was initiated with the addition of free radical initiators and proceeded for 1 h. The molar ratio and the time of reaction reported were optimized to minimize protein aggregation and precipitation, as well as to maximize the solution stability of the resulting NCs (designated below as S—S APO NC). Excess monomers and cross-linkers were removed using ultrafiltration and S—S APO NC was stored in PBS buffer (pH 7.4). DLS clearly showed increase in average diameter of the sample to ~75 nm (Supplement 3) with a slightly positive ζ-potential value of 2.8 mV (Supplement 1). TEM analysis of the S—S APO NC confirmed the nearly doubling in diameter of the spherical particle (Fig. 1e). Unexpectedly, the NCs displayed dark contrast upon uranyl acetate staining, which hints that the cores of the particles were very densely packed. As expected from the incorporation of redox-responsive cross-linker **3**, the reduction of NCs size can be seen upon treatment of the reducing agent glutathione (GSH) (2 mM, 6 h, 37 °C). As shown in Fig. 1f, the densely packed NCs were completely dissociated into ~30 nm particles, confirming the reversible nature of the encapsulation process. As a control, we also synthesized nondegradable MBP—APO NCs (ND APO NC) using *N*,*N*′-methylene bisacrylamide as the cross-linker with same monomer and protein concentrations under identical reaction conditions. Whereas similarly sized NCs were formed, no degradation of ND APO NC can be observed in the presence of GSH.

Cellular uptake and localization of nanocapsules

We next examined the cellular uptake of the S—S APO NC and cellular localization of the cargo. If the unique tumor selectivity of MBP—APO is maintained following the encapsulation and release processes, we expect the delivered MBP—APO to either accumulate in the nuclei of the tumor cells, or to localize in the cytoplasm of noncancerous cells. Prior to the polymerization process, the MBP—APO protein was conjugated to amine-reactive rhodamine (Rho—APO) as described in section 'Protein nanocapsule preparation'. Subsequent encapsulation yielded similarly sized NCs as unlabeled S—S APO NCs. Fluorescent microscopy showed all NCs readily penetrated the cell membrane and are present in the cytoplasm of MDA-MB-231 cells within 1 h (Supplement 4). When the relative amounts of positively charged monomer **2** were reduced in the NC shell, corresponding decreases in ζ-potentials of the NCs were measured by DLS, which led to decreases in cellular internalization (Supplement 5). The cellular trafficking of the internalized S—S Rho—APO NCs in HeLa cells was investigated for 2 h by monitoring colocalization using fluorescent markers for early and late endosomes (Fig. 2a and Supplement 6). Colocalization of Rho—APO with early endosomes was detected at the highest levels after 30 min and decreased at later time points. In contrast, colocalization of Rho—APO with late endosome remained low throughout the trafficking studies. Colocalization of Rho—APO with nuclei became evident after 2 h, indicating endosomal escape and nuclear entry of the released apoptin protein. These results suggested that S—S Rho—APO NCs were trafficked into early endosomes upon internalization and at least a significant portion of the internalized NCs and the cargo can escape from the endosomal compartment.

To analyze protein localization using confocal microscopy, two cancer cell lines HeLa and MCF-7, together with the noncancerous human foreskin fibroblast (HFF), were treated with either S—S Rho—APO NC or ND Rho—APO NC (Fig. 2b). In the case of ND Rho—APO NCs, red fluorescence signals remained in the cytoplasm for all three cell lines, indicating the encapsulated Rho—APO proteins were well-shielded by the nondegradable polymer shell and the internal nuclear localization sequences were not accessible to the transport machinery. In stark contrast, when HeLa cells were treated with S—S Rho—APO NC, strong red fluorescence of rhodamine was present in the nuclei, resulting in intense pink color as a result of overlapping of rhodamine and DAPI fluorescence. Z-stacking analysis confirmed the Rho—APO to be localized inside of the nuclei. Similar results were observed with MCF-7 cells, although the fluorescence intensity was not as strong as in the HeLa cells. These results confirmed that the Rho—APO delivered can indeed be released in native forms inside the cytoplasm and enter the nuclei. More importantly, the tumor-specificity of delivered apoptin proteins toward cancer cell lines were demonstrated in the confocal analysis of noncancerous HFF cells treated with S—S Rho—APO NC, as all of the dye signals remained in the cytoplasm and no nuclear accumulation was observed.

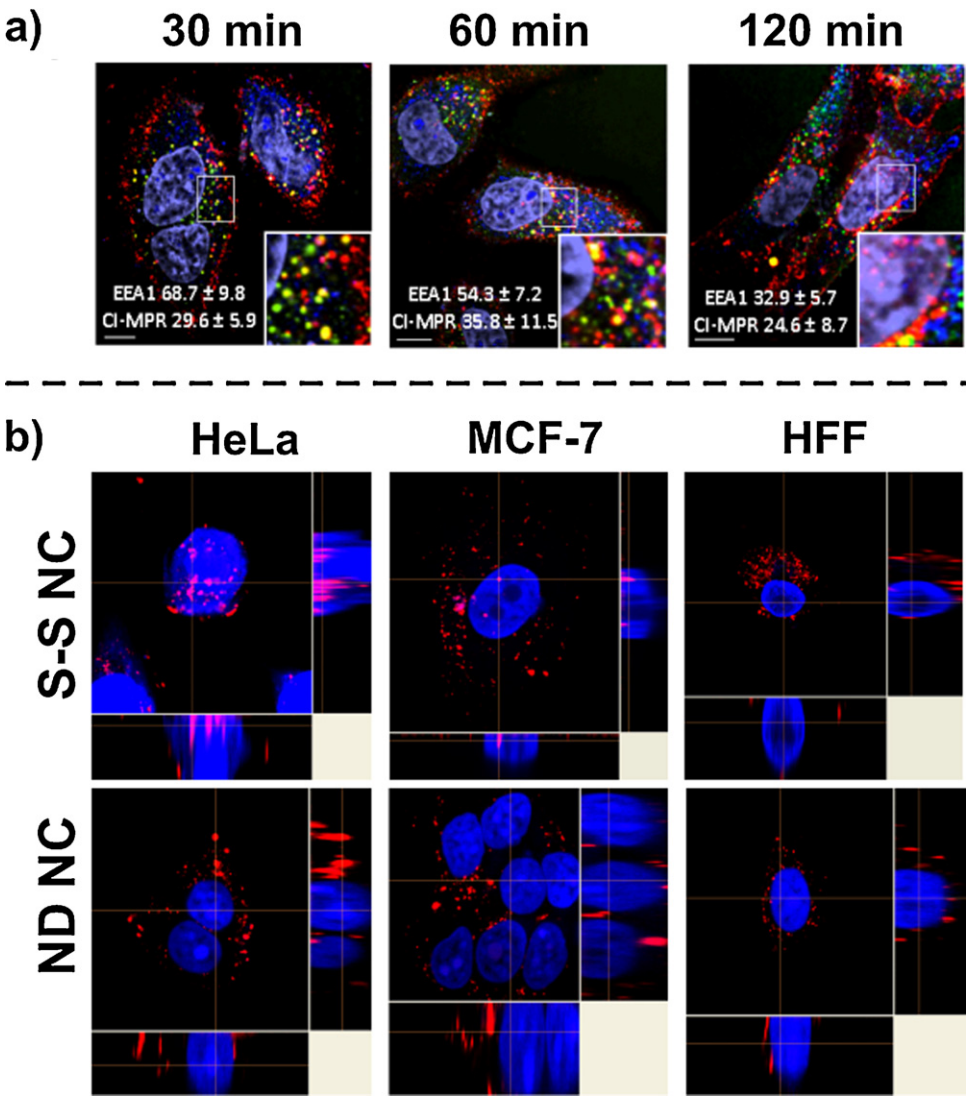

Figure 2 Protein nanocapsule cellular trafficking and localization. (a) The trafficking of Rho—APO in S—S NCs through endosomes. HeLa cells were incubated with 20 nM S—S Rho—APO NCs (red) at 37 °C for various time periods, 30, 60 and 120 min. Early endosomes were detected by early endosome antigen 1 (EEA1, green). Late endosomes were detected by cation-independent mannose-6-phosphate receptor (CI-MPR, blue). Nuclei were stained with DAPI and shown as purple. The scale bar represents 10 μm. The percentage of fluorescence colocalization was quantified by calculating colocalization coefficients using Manders' overlap coefficient (>10 samples) and shown in each figure; (b) confocal microscopy of cellular localization of Rho—APO encapsulated in S—S NC and ND NC to cancer cell lines HeLa and MCF-7, and noncancerous HFF. Nuclei were stained with DAPI (blue). The scale bar is 20 μm.

Tumor-selective cytotoxicity of apoptin nanocapsules

We then investigated whether the MBP—APO protein delivered still possesses its function to induce tumor-selective apoptosis. The potency and selectivity of S—S APO NC were tested on various cell lines including HeLa, MCF-7, MDA-MB-231, and HFF (Fig. 3a—d). MTS assay was used to measure cell viability 48 h after addition of the protein and NC. For each cell line, ND APO NC and native MBP—APO were used as negative controls. When S—S APO NC was added to a final concentration of 200 nM, all three cancer cell lines had no viable cells, whereas ~75% of the HFF had survived. The IC_{50} values were 80 and 30 nM for HeLa and MDA-MB-231, respectively. The IC_{50} for MCF-7 was higher at ~110 nM, which may be due to the deficiency in the terminal executioner caspase 3 and reliance on other effector caspases for apoptosis [29,30]. As expected, native MBP—APO and ND APO NC did not significantly decrease the viability of any cell lines tested, consistent with the inability to enter cells and release MBP—APO in cytoplasm, respectively. The IC_{50} values of S—S APO NC toward MDA-MB-231 increased as the surface charge of the NC became more neutral (Supplement 5), suggesting more efficient internalization can improve S—S NCs cytotoxicity. The morphologies of MDA-MB-231 and HFF cells were examined under various treatments. Only the S—S APO NC treated MDA-MB-231 cells exhibited blebbing and shrinkage, which are hallmarks of apoptotic cell death (Fig. 3e

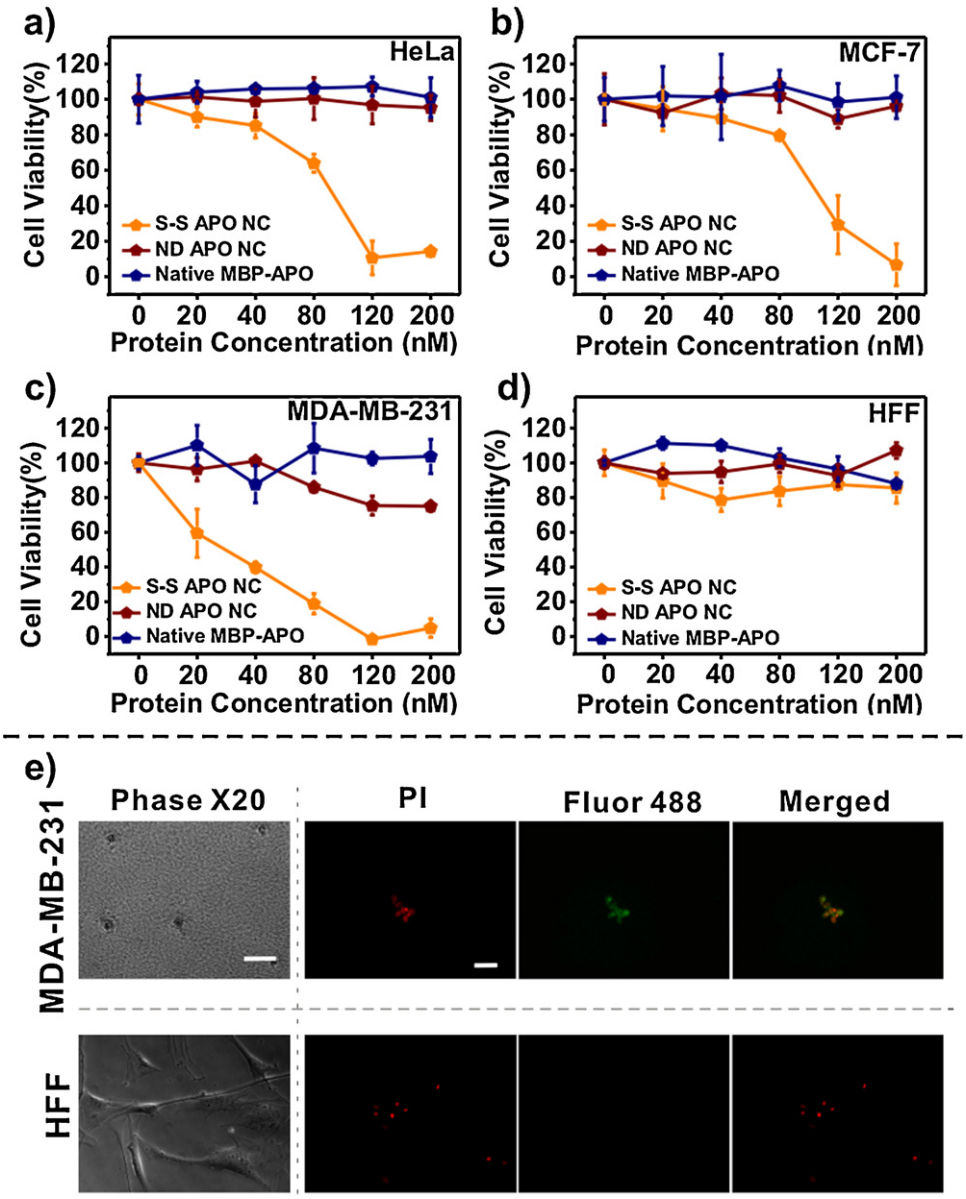

Figure 3 Cytotoxicity and apoptosis observed following nanocapsule delivery. (a) HeLa; (b) MCF-7; (c) MDA-MB-231; or (d) HFF cells with treatment of different concentrations of S—S APO NC, ND APO NC, and native MBP—APO. (e) Apoptosis induced by S—S APO NC determined by TUNEL assay. Images on the left are bright field microscopy images of MDA-MB-231 and HFF cells treated for 24 h with 200 nM S—S APO NC. The scale bar represents 50 μm. Images right of the dash line shows detection of apoptotic fragmentation of the nucleosome after same treatment using APO-BrdU™ TUNEL assay kit. The scale bar represents 50 μm. Red fluorescence represents the propidium-iodide (PI)-stained total DNA, and green fluorescence represents the Alexa Fluor 488-stained nick end label, the indicator of apoptotic DNA fragmentation. The merged pictures combine the PI-stained nuclei and the Alexa Fluor 488-stained nick end label. (Note the bright field images do not overlap with the fluorescent microscopy images; cells were detached and collected for TUNEL assay after treatment.)

and Supplement 7). Using TUNEL assay, S—S APO NC treated MDA-MB-231 also showed nuclear fragmentation associated with apoptosis, whereas cells treated with native MBP—APO and ND APO NC at the same concentration (Supplement 7), as well as HFF treated with 200 nM S—S APO NC (Fig. 3e), had no sign of apoptosis. Collectively, these results demonstrated that the recombinant MBP—APO delivered by the degradable NCs retains the potency and selectivity as the transgenically expressed apoptin in previous studies [9].

In vivo evaluation of apoptin nanocapsules

We further examined the potency of S—S APO NC in a mouse xenograft model. Female athymic nude (*nu*/*nu*) mice were subcutaneously grafted on the back flank with 5×10^6 MCF-7 breast cancer cells. When the tumor volume reached 100—200 mm^3 (day 0), mice were randomly separated into different groups and treated with intratumoral injection of PBS, MBP—APO, S—S APO NC. In addition, S—S NC with bovine serum albumin (S—S BSA NC) was added as a nonlethal

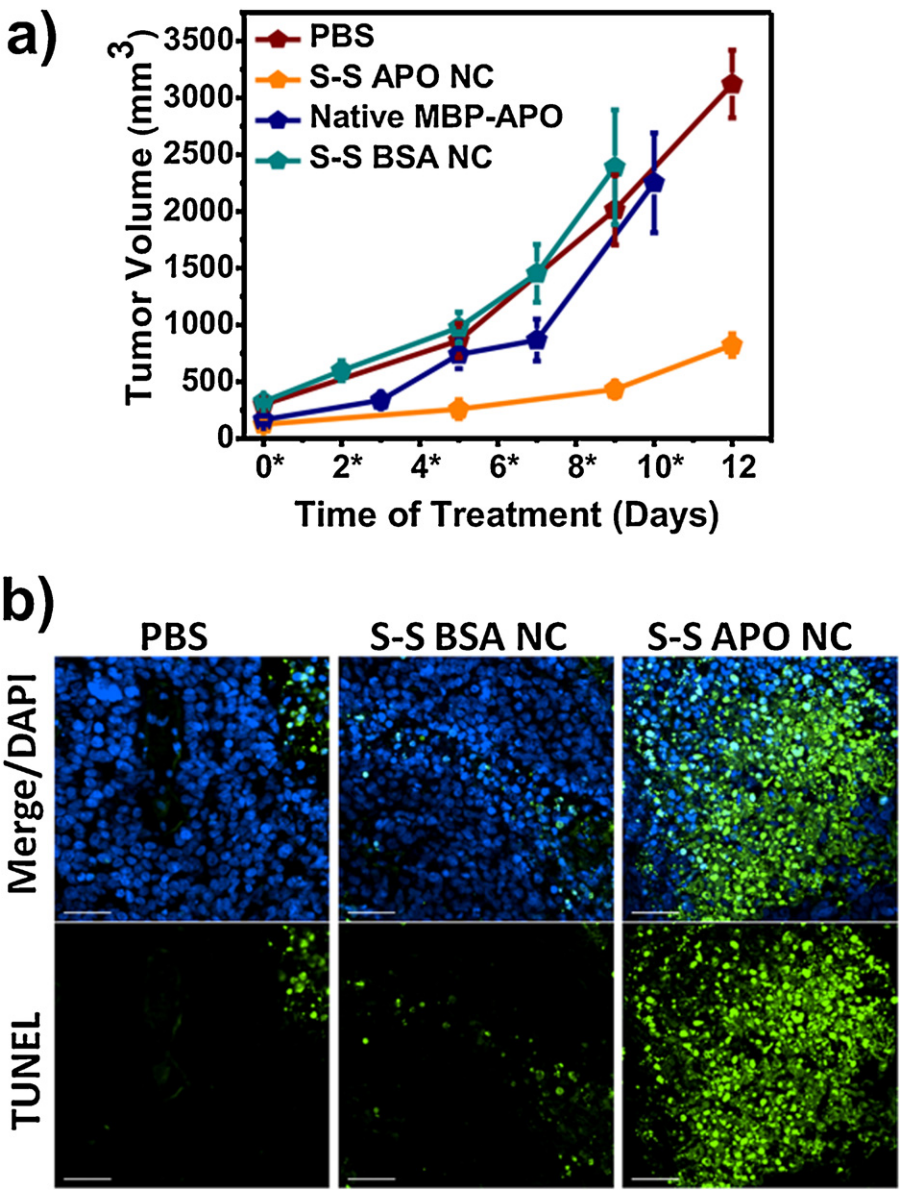

Figure 4 Treatment of apoptin nanocapsules resulted in tumor growth retardation. (a) Significant tumor inhibition was observed in the mice treated by S—S APO NC. Female athymic nude mice were subcutaneously grafted with MCF-7 cells and treated with intratumoral injection of MBP—APO ($n = 4$) or S—S APO NC ($n = 4$) (200 μg/mouse) every other day. PBS ($n = 3$) and S—S BSA NC ($n = 4$) were included as negative controls. The average tumor volumes were plotted *vs.* time. Asterisks indicate injection days. (b) Detection of apoptosis in tumor tissues after treatment with different NCs. Cross-sections of MCF-7 tumors were stained with fluorescein-dUTP (green) for apoptosis and DAPI for nucleus (blue). The scale bars represent 50 μm.

protein cargo control to test the effects of the S—S NC polymer component on tumor cells *in vivo*. Tumors treated with saline, S—S BSA NC or native MBP—APO expanded rapidly and reached the maximum limit (>2500 mm^3) within 12 days. In sharp contrast, tumor growth was significantly delayed when treated with S—S APO NC (Fig. 4a). Fixed tumor tissues collected from each treatment group were examined for DNA fragmentation using *in situ* TUNEL assay. The images revealed the highest level of cell apoptosis for the tumor harvested from mice treated with S—S APO NC, correlating well with the significantly delayed tumor growth observed for this treatment group and confirming that tumor growth inhibition was indeed due to apoptin-mediated apoptosis (Fig. 4b). Collectively, the xenograft study verified that the degradable NCs effectively delivered MBP—APO proteins to tumor cells *in vivo*, which was highly effective in limiting tumor progression. Upon further optimization of the pharmacokinetics of the S—S APO NC, including surface derivatization with active targeting ligands, these particles may be intravenously administered as an anticancer therapy [31].

Conclusions

We were able to deliver the high molecular weight complex of the tumor-selective MBP—APO using a redox-responsive polymeric NC *in vitro* and *in vivo*. The choice and design

of the sub-100 nm NC is well-suited for diverse protein targets because of its mild preparation conditions, reversible encapsulation, efficient membrane penetration, and cytoplasmic release of the protein cargo. Our application here further illustrates how intracellular protein delivery using nanoscale system can provide new possibilities for achieving selective anticancer therapy.

Acknowledgements

This work was supported by a David and Lucile Packard Foundation to Y.T.; a CDMRP BCRP Idea Award BC101380 to Y.T. and P.W. We thank Dr. C. Backendorf and Dr. M. Noteborn (Universiteit Leiden) for the expression plasmid of MBP—APO.

Appendix A. Supplementary data

Supplementary data associated with this article can be found, in the online version, at http://dx.doi.org/10.1016/j.nantod.2012.12.003.

References

[1] J.B. Gibbs, Science 287 (2000) 1969.
[2] J.H. Atkins, L.J. Gershell, Nat. Rev. Drug Discov. 1 (2002) 491.
[3] G.I. Evans, K.H. Vousden, Nature 411 (2001) 342.
[4] J.C. Reed, Cancer Cell 3 (2003) 17.
[5] T.G. Cotter, Nat. Rev. Cancer 9 (2009) 501.
[6] A. Russo, M. Terrasi, V. Agnese, D. Santini, V. Bazan, Ann. Oncol. 17 (2006) 115.
[7] C.J. Brown, S. Lain, C.S. Verma, A.R. Fersht, D.P. Lane, Nat. Rev. Cancer 9 (2009) 862.
[8] M.H.M. Noteborn, Eur. J. Pharmacol. 625 (2009) 165.
[9] C. Backendorf, A.E. Visser, A.G. de Boer, R. Zimmerman, M. Visser, P. Voskamp, Y.H. Zhang, M. Noteborn, Annu. Rev. Pharmacol. Toxicol. 48 (2008) 143.
[10] M. Los, S. Panigrahi, I. Rashedi, S. Mandal, J. Stetefeld, F. Essmann, K. Schulze-Osthoff, Biochim. Biophys. Acta 1793 (2009) 1335.
[11] S.M. Zhuang, A. Shvarts, H. van Ormondt, A.G. Jochemsen, A.J. van der Eb, M.H. Noteborn, Cancer Res. 55 (1995) 486.
[12] J.G. Teodoro, D.W. Heilman, A.E. Parker, M.R. Green, Genes Dev. 18 (2004) 1952.
[13] A.A.A.M. Danen-Van Oorschot, D.F. Fischer, J.M. Grimbergen, B. Klein, S.M. Zhuang, J.H.F. Falkenburg, C. Backendorf, P.H.A. Quax, A.J. Van der Eb, M.H.M. Noteborn, Proc. Natl. Acad. Sci. U.S.A. 94 (1997) 5843.
[14] S.R. Leliveld, Y.H. Zhang, J.L. Rohn, M.H. Noteborn, J.P. Abrahams, J. Biol. Chem. 278 (2003) 9042.
[15] A.A.A.M. Danen-Van Oorschot, Y.H. Zhang, S.R. Leviveld, J.L. Rohn, M.C.M.J. Seelen, M.W. Bolk, A. van Zon, S.J. Erkeland, J.P. Abrahams, D. Mumberg, M.H.M. Noteborn, J. Biol. Chem. 278 (2003) 27729.
[16] J.L. Rohn, Y.H. Zhang, R.I. Aalbers, N. Otto, J. Den Hertog, N.V. Henriquez, C.J. Van De Velde, P.J. Kuppen, D. Mumberg, P. Donner, M.H. Noteborn, J. Biol. Chem. 277 (2002) 50820.
[17] A.M. Pietersen, M.M. van der Eb, H.J. Rademaker, D.J. van den Wollenberg, M.J. Rabelink, P.J. Kuppen, J.H. van Dierendonck, H. van Ormondt, D. Masman, C.J. van de Velde, A.J. van der Eb, R.C. Hoeben, M.H. Noteborn, Gene Ther. 6 (1999) 882.
[18] M.M. van der Eb, A.M. Pietersen, F.M. Speetjens, P.J. Kuppen, C.J. van de Velde, M.H. Noteborn, R.C. Hoeben, Cancer Gene Ther. 9 (2002) 53.
[19] D.J. Peng, J. Sun, Y.Z. Wang, J. Tian, Y.H. Zhang, M.H. Noteborn, S. Qu, Cancer Gene Ther. 14 (2007) 66.
[20] M.L. Edelstein, M.R. Abedi, J. Wixon, J. Gene Med. 9 (2007) 833.
[21] L. Guelen, H. Paterson, J. Gaken, M. Meyes, F. Farzaneh, M. Tavassoli, Oncogene 23 (2004) 1153.
[22] J. Sun, Y. Yan, X.T. Wang, X.W. Liu, D.J. Peng, M. Wang, J. Tian, Y.Q. Zong, Y.H. Zhang, M.H.M. Noteborn, S. Du, Int. J. Cancer 124 (2009) 2973.
[23] C. Murriel, S. Dowdy, Expert Opin. Drug Deliv. 3 (2006) 739.
[24] J. Shi, A.R. Votruba, O.C. Farokhzad, R. Langer, Nano Lett. 10 (2010) 3223.
[25] Z. Gu, A. Biswas, M. Zhao, Y. Tang, Chem. Soc. Rev. 40 (2011) 3638.
[26] P.P. Adiseshaiah, J.B. Hall, S.E. McNeil, Nanomed. Nanobiotechnol. 2 (2010) 99.
[27] Z. Gu, M. Yan, B. Hu, K.I. Joo, A. Biswas, Y. Huang, Y. Lu, P. Wang, Y. Tang, Nano Lett. 9 (2009) 4533.
[28] M. Zhao, A. Biswas, B.L. Hu, K.I. Joo, P. Wang, Z. Gu, Y. Tang, Biomaterials 32 (2011) 5223.
[29] M. Burek, S. Maddika, C.J. Burek, P.T. Daniel, K. Schulze-Osthoff, M. Los, Oncogene 25 (2006) 2213.
[30] R.U. Janicke, M.L. Sprengart, M.R. Wati, A.G. Porter, J. Biol. Chem. 273 (1998) 9357.
[31] N. Kamaly, Z. Xiao, P.M. Valencia, A.F. Radovic-Moreno, O.C. Farokhzad, Chem. Soc. Rev. 41 (2012) 2971.

Muxun Zhao obtained her B.S. degree in Biochemistry, Biology and Biotechnology from Worcester Polytechnic Institute in 2009. She then joined the Department of Chemical and Biomolecular Engineering at University of California, Los Angeles for graduate studies. She is now a fourth year Ph.D. student in Professor Yi Tang's laboratory. Her current research interests include bionanotechnology and biomaterials towards cancer treatment.

Biliang Hu received his B.S. in Biology at University of Science and Technology of China in 2007. He is currently a Ph.D. student in Department of Chemical Engineering and Materials Science at University of Southern California. He has worked on various research topics, ranging from dendritic cell-directed lentiviral vectors for cancer vaccines, biodegradable polymer matrix for immune modulation, nanoparticles for protein delivery, peptide design towards high stability and efficient oral availability, and antibody-directed modulation of tumor microenvironment.

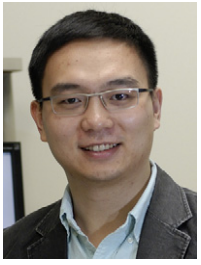

Dr. Zhen Gu obtained his Ph.D. degree in 2010, with a major in MEMS and nanotechnology at University of California, Los Angeles, under the guidance of Prof. Yi Tang in the Department of Chemical and Biomolecular Engineering. He was a postdoctoral associate working with Prof. Robert Langer at Massachusetts Institute of Technology and Harvard Medical School during 2010 to 2012. He is currently an assistant professor in the joint Department of Biomedical Engineering at University of North Carolina at Chapel Hill and North Carolina State University. He also holds an adjunct position in the UNC Eshelman School of Pharmacy. His research interests include controlled drug delivery, bio-inspired materials, implantable devices and biochip technology.

Dr. Kye-Il Joo, Ph.D., is currently a postdoctoral research associate at Department of Chemical Engineering and Materials Science, University of Southern California. He obtained his B.S. from Hanyang University, Korea (2002) and Ph.D. from Viterbi School of Engineering, University of Southern California (2009). He has a broad training in biochemical engineering, nanotechnology, biomaterials, and immunobioengineering. His recent research is focused on the design of crosslinked multilamellar liposomal nanoparticles for controlled release of anticancer drugs, as well as the design of biodegradable hydrogels to modulate immune cells for enhanced vaccination.

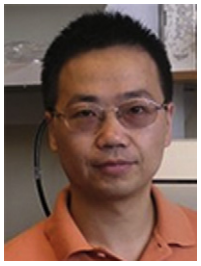

Dr. Pin Wang is an associate professor in the Department of Chemical Engineering and Materials Science, Department of Biomedical Engineering, and Department of Pharmacology and Pharmaceutical Science at University of Southern California (USC). He received his Ph.D. in 2003 from California Institute of Technology (Caltech). After a postdoctoral study at Caltech, he joined USC as an assistant professor in 2005. Dr. Wang's research focuses on engineering viral vectors for targeted gene delivery, dendritic cell-directed vaccines against cancers and infectious disease, tumor microenvironment, and design of nanoparticles for drug delivery.

Dr. Yi Tang obtained his B.S. degrees in Chemical Engineering and Material Science from Penn State University in 1997. He then moved to California Institute of Technology and studied biopolymer biosynthesis under the guidance of Prof. David A. Tirrell. After obtaining his Ph.D. in 2002, he moved to Stanford University to study biosynthesis with Prof. Chaitan Khosla. In 2004, he began his independent academic career in the Department of Chemical and Biomolecular Engineering at the University of California, Los Angeles, where he is now the Chancellor's Professor. He currently holds a joint appointment in the Department of Chemistry and Biochemistry. His group studies bionanotechnology, natural product biosynthesis and biocatalysts.

Clickable Protein Nanocapsules for Targeted Delivery of Recombinant p53 Protein

Journal:	*Journal of the American Chemical Society*
Manuscript ID:	ja-2014-08083g.R1
Manuscript Type:	Article
Date Submitted by the Author:	19-Sep-2014

Complete List of Authors:	Zhao, Muxun; University of California, Los Angeles, Chemical and Biomolecular Engineering Liu, Yarong; University of Southern California, Department of Chemical Engineering and Materials Science Hsieh, Renee; University of California, Los Angeles, Chemical and Biomolecular Engineering Wang, Nova; UCLA, Tai, Wanyi; University of Washington, Bioengineering Joo, Kye-Il; University of Southern California, Department of Chemical Engineering and Materials Science Wang, Pin; University of Southern California, Department of Chemical Engineering and Materials Science Gu, Zhen; University of North Carolina at Chapel Hill / NC State University, Joint Biomedical Engineering/UNC Molecular Pharmaceutics Tang, Yi; University of California, Los Angeles, Chemical and Biomolecular Engineering

Clickable Protein Nanocapsules for Targeted Delivery of Recombinant p53 Protein

Muxun Zhao[1], Yarong Liu[2], Renee S. Hsieh[1], Nova Wang[1], Wanyi Tai[3], Kye-Il Joo[2], Pin Wang[2], Zhen Gu[3], Yi Tang[1]*

[1] Department of Chemical and Biomolecular Engineering, Department of Chemistry and Biochemistry, University of California, Los Angeles, CA 90095, USA; [2] Mork Family Department of Chemical Engineering and Materials Science, University of Southern California, Los Angeles, CA 90089, USA; [3] Joint Department of Biomedical Engineering, University of North Carolina at Chapel Hill, North Carolina State University, Raleigh, NC 27695, USA

Protein delivery, tumor targeting, click chemistry, redox-sensitive, tumor suppressor, luteinizing hormone-releasing hormone

ABSTRACT: Encapsulating anticancer protein therapeutics in nanocarriers is an attractive option to minimize active drug destruction, increase local accumulation at disease site and decrease side effects to other tissues. Tumor specific ligands can further facilitate in targeting the nanocarriers to the tumor cells and reduce nonspecific cellular internalization. Rationally designed non-covalent protein nanocapsules, incorporating copper-free "click chemistry" moiety, polyethylene glycol (PEG) unit, redox-sensitive crosslinker, and tumor specific targeting ligand, have been synthesized to selectively deliver intracellular protein therapeutics into tumor cells via receptor-mediated endocytosis. These nanocapsules can be conjugated to different targeting ligands of choice, such as anti-Her2 antibody single-chain variable fragment (scFv) and luteinizing hormone releasing hormone (LHRH) peptide, which result in specific and efficient accumulation within tumor cells overexpressing corresponding receptors. LHRH-conjugated nanocapsules selectively delivered recombinant human tumor suppressor protein p53 and its tumor-selective super variant into targeted tumor cells, which led to reactivation of p53-mediated apoptosis. Our results validate a general approach for targeted protein delivery into tumor cells using cellular-responsive nanocarriers, opening up new opportunity for the development of intracellular protein-based anticancer treatment.

Virtually all human cancer cells have elaborate anti-apoptotic strategies to overcome apoptosis, which is a vital cellular mechanism to obstruct tumor progression.[1] The most commonly mutated gene in tumor cells is the tumor suppressor gene *TP53*, the protein product of which promotes apoptosis of aberrant cells through both transcription-dependent and independent mechanisms.[2] In this manner, the genome guardian p53 is critically important in eliminating possible neoplastic cells incurred during DNA damage. About 50% of all the human tumors have mutant p53 proteins.[3] Therefore, restoring p53 function can be a highly effective option for cancer treatment. Functional copies of p53 can not only resurrect the apoptotic circuitry, but also sensitize the tumor cells towards other various treatments (radio- and chemotherapy).[4] Different strategies pursuing this goal have been intensively investigated, including small molecules and peptides that overcome p53 mutations, as well as adenovirus/p53 gene delivery vectors.[5-8] While restoring p53 functions in cancer cells has been a tantalizing approach towards combating cancer, the lack of effective delivery method has undermined its potential as an anti-cancer therapeutic.

Intracellular protein delivery using stimuli-responsive nanomaterials has emerged as an attractive method to deliver various cargos to the cells of interest.[9-18] In particular, water soluble polymer-based nanocarriers that encapsulate the protein of interest to aid the penetration of cellular membrane, while capable of releasing the protein upon various cellular stimuli, have been demonstrated to be effective in functional delivery of proteins.[19] Nanocarriers that can be triggered to release protein cargo in response to changes in temperature, light, pH, redox potential and enzymatic activities have been reported.[9,20-23] As a result, nanocapsules-mediated delivery of recombinant p53 to cancer cells may be a direct method of reactivating the apoptosis pathway and inducing programmed cell death. One critical limitation of previous protein-containing nanocapsule is that the polymer layer is synthesized from a positively charged monomer that enables nonselective entry across cellular membrane. However, since the level of p53 is tightly regulated in normal cells, targeted delivery of p53 using functionalized nanocapsules that restricts entry to only cancer cells is highly desirable. Hence, new nanocapsule encapsulation strategy that allows facile modification of the polymeric carrier is needed.

To equip the nanocapsules with cancer-targeting ligands such as peptides and antibodies that can enable receptor mediated endocytosis, the surface of the nanocapsules must be decorated with reactive handles that facilitate aqueous-based conjugation chemistry. The chemistry utilized must be nondenaturing to maintain the native form of protein cargo. This is especially important for p53 delivery since the protein forms a tetrameric complex that is prone to aggregation and loss of function.[24] The reaction must also be orthogonal to the nanocapsule synthesis chemistry and compatible with the designed degradation mechanism of the polymer capsule, such as disulfide mediated redox-sensitive degradation. One of the most versatile reactions that are compatible with a protein-based cargo is the copper-free click chemistry that utilizes azides and aryl cyclooctynes.[25-27] Click chemistry has been used for modification of nanoparticles for direct conjugation of ligands and

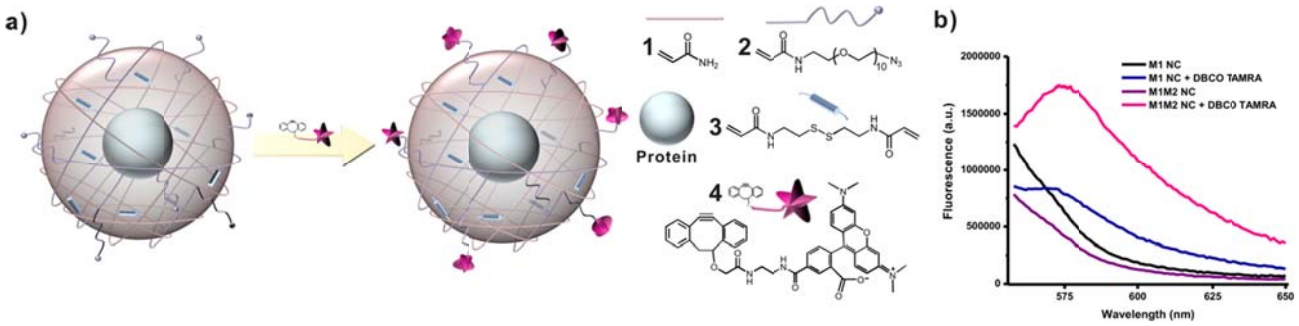

Figure 1. Clickable nanocapsules. **a**) Schematic diagram of clickable, redox-sensitive protein nanocapsules, and scheme of conjugation to DBCO TAMRA using copper-free click chemistry. **b**) Fluorescence spectra of NC samples before and after copper-free click conjugation to DBCO TAMRA.

chromophores.[28,29] In this report, we demonstrate that pegylated protein nanocapsules containing reactive azidogroups on the surface can be synthesized, which allows facile conjugation to various tumor-targeting ligands. More importantly, we show that recombinant p53 can be selectively delivered to cancer cells using nanocapsules clicked with specific targeting ligand.

RESULTS AND DISCUSSIONS

Synthesis of nanocapsules with clickable monomer

Our synthesis strategy for protein nanocapsules is shown in Figure 1. Monomers and redox-sensitive crosslinkers can deposited at the surface of the protein via van der Waals interactions, and can be polymerized *in situ* around the target protein to form a non-covalent shell that encapsulates the protein. The monomer acrylamide (**1**) is used as a general building block of the water-soluble shell. The nanocapsules are crosslinked with *N,N'*-bis(acryloyl)cystamine (**3**), which is designed to degrade in highly reducing environments such as the cytoplasm,[30] thereby releasing the protein cargo intracellularly. To synthesize a near-neutral polymer shell that does not enter cells via positive charges, we first eliminated the use of positively charged monomers employed in previous designs, such as *N*-(3-aminopropyl)methacrylamide. Instead, we chose *N*-(azidoethyl-decaethylene glycol)-acrylamide (**2**) as the second monomer (Figure 1a). The neutral **2** contains a terminal azido group that can be used as the reactive site for cross-coupling via copper-free click reaction. The ten ethylene glycol units serve as a water soluble spacer at the surface of the nanocapsules, and provide flexibility to the conjugated targeting ligands. Through copolymerization of **1** and **2**, the azido functionalities can be displayed on the surface of the nanocapsules for subsequent modification. Monomer **2** was readily prepared by reacting *O*-(2-aminoethyl)-*O'*-(2-azidoethyl)nonaethylene glycol with acryloyl chloride.[29] After purification and MS characterization of monomer **2** (Figure S1), we first performed the *in situ* polymerization process using green fluorescent protein (GFP) as the cargo. Following one hour of polymerization during which the mole fraction of **2** was 1.5% of total monomers, uniformly sized nanocapsules were synthesized, with an electrostatic potential of ~ -0.9 mV, and an average size of 9.1±0.8 nm (PDI = 0.32) To examine the structural integrity of the encapsulated proteins, we performed circular dichroism measurement on both free GFP protein and GFP containing nanocapsules. As expected, no significant change to the secondary structure of GFP was observed upon encapsulation (Figure S2).

To verify the presence of azido groups on the surface of the nanocapsules, we performed the copper-free reaction between dibenzylcyclooctyne TAMRA (DBCO TAMRA, **4**) and the GFP nanocapsules prepared from monomers **1** and **2.** As a control, nanocapsules synthesized from **1** alone were also mixed with **4**. After overnight stirring at 4°C, the reaction was subjected to repeated dialysis and ultrafiltration (30K MWCO) to remove any unreacted **4**. The conjugation of TAMRA to the protein nanocapsules was detected by fluorescence emission scan (Figure 1b). Whereas nanocapsules synthesized with both **1** and **2** exhibited the characteristic emission peak at 580 nm of TAMRA, the control sample with only **1** showed nearly no additional signal at the same wavelength compared to negative controls. Given the measured differences in hydrodynamic radius (R_h) between the GFP nanocapsules (4.5 nm) and free GFP (2.5 nm), we estimate no more than three GFP can be packed into each nanocapsule. We previously established by experiments that most of the nanocapsules prepared via the interfacial polymerization method contain a single copy of GFP.[31] Taking together, the nanocapsules synthesized here should contain either one or two GFP molecules. The number of TAMRA molecules conjugated per nanocapsule was approximated by comparing of relative intensities of GFP and TAMRA fluorescence. Given the above estimation of one to two GFP per nanocapsule, we approximated that each nanocapsule was conjugated with four to eight TAMRA molecules through the click reaction with accessible azido functional groups.

Conjugation of nanocapsules with targeting ligands

After confirming the successful "clicking" of cyclooctyne moieties onto the surface of azido-functionalized nanocapsules, we then developed methods to conjugate cancer targeting ligands. We first selected the luteinizing hormone releasing hormone (LHRH) peptide **5** (Glp-His-Trp-Ser-Tyr-D-Lys-Leu-Arg-Pro-NHEt, Figure 2a), which binds to LHRH receptors that are overexpressed in various hormonal related cancers, such as breast and prostate cancers.[32] LHRH receptors are not expressed detectably in most visceral organs and have been targeted in the delivery of small molecules.[33,34] The bifunctional dibenzocyclooctyne-PEG4-N-hydroxysuccinimidyl ester (DBCO-PEG4-NHS ester, **6**) was chosen as the tether (Figure 2a). The peptide **5** was first conjugated to the NHS terminus of **6** through the internal D-Lys designed to serve as a site for coupling. The adduct **7** was verified by LC-MS and purified by HPLC to homogeneity (Figure S3). Subsequently, **7** was added to the azido-functionalized GFP nanocapsules at a molar ratio of 15:1 and allowed to react overnight at 4°C. Following the click reaction, unreacted **7** was removed through ultrafiltration (30K MWCO) and the nanocapsules were dialyzed into phosphate-buffered saline. To test the LHRH receptor mediated endocytosis of nanocapsules, we added the LHRH functionalized

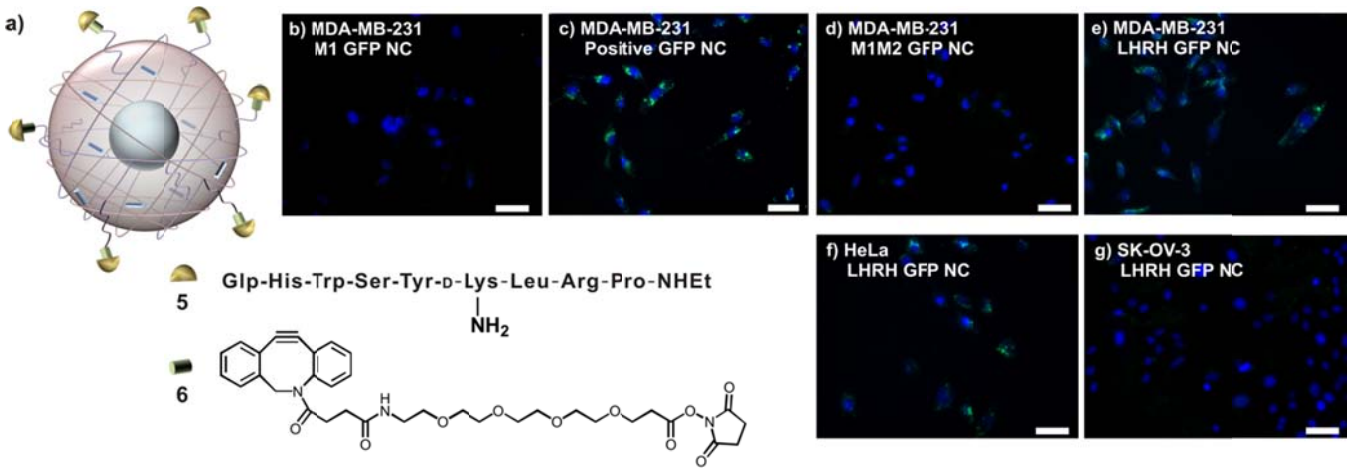

Figure 2. Selective internalization of LHRH conjugated nanocapsules. **a**) Scheme of LHRH S-S nanocapsule. Glp is cyclized glutamine; **b-g**) Fluorescence microscopy images of cell lines treated with 400 nM GFP-containing nanocapsules. **b**) MDA-MB-231 treated with GFP nanocapsules synthesized with monomer **1** alone; **c**) MDA-MB-231 treated with positively charged GFP nanocapsule; **d**) MDA-MB-231 treated with GFP nanocapsules synthesized from monomers **1** and **2** (no targeting ligand); **e**) MDA-MB-231 treated with GFP nanocapsules synthesized from monomers **1** and **2** and conjugated with the LHRH targeting ligand); **f**) HeLa cells treated with nanocapsules in **e; g**) SK-OV-3 cells treated with nanocapsules in **e**. Nuclei were stained with DAPI (blue). The scale bars represent 50 μm.

nanocapsules to MDA-MB-231 cells, which is known to overexpress the receptor.[35] As controls we also added GFP nanocapsules that are i) positively charged and are expected to be internalized (synthesized from monomers **1** and *N*-(3-aminopropyl)methacrylamide); ii) azido-functionalized but not conjugated to LHRH (synthesized from monomers **1** and **2**); and iii) do not contain azido groups (synthesized from monomer **1** only). After overnight incubation, the internalization of nanocapsules was visualized by fluorescence microscopy.

As can be seen from Figure 2c, the positively charged nanocapsules were well-internalized as expected. In contrast, the neutral nanocapsules, either with or without azido groups, were not internalized into cells at all. LHRH-functionalized GFP nanocapsules, however, were efficiently internalized as can be seen from the GFP fluorescence in the cytoplasm. To quantify the extent of internalization through LHRH receptor, flow cytometry measurement was performed on samples as shown in Figure 3a. The level of internalization through LHRH receptor mediated endocytosis is ~70% of that observed with positively charged nanocapsules. More importantly, azido-functionalized nanocapsules without LHRH conjugation did not exhibit noticeable internalization compared to no treatment or native GFP controls. Trafficking experiments were performed for the LHRH-targeted GFP nanocapsules (Figure 3bc). Localization in the early endosomes was observed within 30 minutes, while release into the cytoplasm was detected at one and two hours after delivery. No significant localization of GFP in the late endosome was observed.

To further test the selectivity of the protein delivery, we added the LHRH-functionalized nanocapsules to several cell lines with varying expression levels of LHRH receptor. When added to cervical cancer cell line HeLa cells that have comparable levels of expression, the amount of internalization were similar to that of MDA-MB-231(Figure 2f). No internalization was seen with the SK-OV-3, which is a LHRH receptor-negative ovarian cancer cell line (Figure 2g).[36] We then examined the targeting and internalization of the LHRH-targeted GFP nanocapsules after exposing them in FBS containing DMEM media at 37˚C for 24 and 48 hours. No attenuation in internalization was observed compared to untreated nanocapsules, suggesting the targeting mechanism remained intact and the nanocapsules were stable under serum-like conditions (Figure S5).

To demonstrate the versatility of the surface functionalization, we conjugated the single-chain variable fragment (scFv) of the anti-Her2 antibody to the azido-functionalized GFP nanocapsules. A maleimide containing bifunctional linker was used to react with cysteine residue on the recombinant scFv (linker to antibody molar ratio of 5:1) (Figure S6). The extent of conjugation was calculated based on the relative protein concentrations of scFv and GFP in the HER2-conjugated GFP nanocapsules. The total protein concentration of the anti-HER2 scFv conjugated GFP nanocapsules was first determined by the Bradford method, and the concentration of GFP was determined by measuring the fluorescence of the nanocapsules, which can correlate to GFP concentration using a standard line (Figure S6). The difference between total protein concentration and GFP concentration is then attributed to the conjugated anti-HER2 scFv. The ratio of anti-HER2 scFv to GFP concentration gives the number of conjugated scFv per GFP containing nanocapsule. When the scFv to protein nanocapsule molar ratio was at 10:1, the number of scFv was estimated to be three to six assuming either one or two GFP per nanocapsule, respectively. When administered to various cell lines, internalization of GFP was only observed in SK-BR-3 that overexpresses the HER2 receptor, and no fluorescence was seen in triple negative breast cancer cell line MDA-MB-231, HeLa or human foreskin fibroblasts (HFF) (Figure S6). Collectively these data illustrate the polymerization, conjugation and internalization steps are all effective as designed.

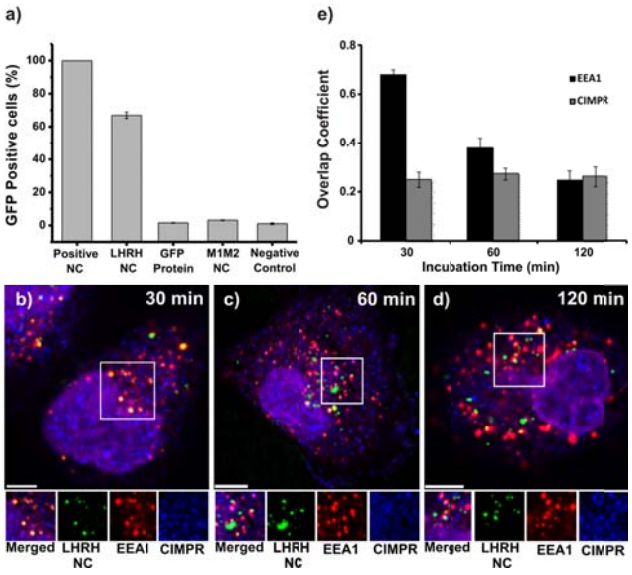

Figure 3. Cellular uptake and trafficking of LHRH nanocapsules by MDA-MB-231 cells. **a**) Cellular internalization of 400 nM GFP protein or nanocapsules by MDA-MB-231 cells at 37°C for 12 hours. The mean fluorescence intensity was measured by flow cytometry and was represented as the percentage of fluorescence from MDA-MB-231 cells incubated with positively charged nanocapsules. **b-d**) The trafficking of LHRH-conjugated GFP nanocapsules through endosomes. MDA-MB-231 cells were incubated with 800 nM nanocapsules at 37°C for various time periods, 30, 60 and 120 min. Early endosomes were detected by early endosome antigen 1 (EEA1, green). Late endosomes were detected by cation-independent mannose-6-phosphate receptor (CI-MPR, blue). Nuclei were stained with DAPI and shown as purple. The scale bar represents 10 μm. **e**) Quantification of LHRH-conjugated GFP nanocapsules colocalized with EEA1 or CI-MPR at various incubation time points. Colocalization coefficients were calculated using Manders' overlap coefficient (>10 samples). The error bars indicate standard deviation.

Synthesis of clickable p53 nanocapsules

We then applied the nanocapsule synthetic steps towards the targeted delivery of p53 to cancer cells. Delivery of recombinant p53 poses significant challenges as the tetrameric complex can readily aggregate and lose activity under non-native condition.[37] The three-dimensional structure of p53 is also not well resolved, and has been shown to be loosely organized, especially in the absence of DNA.[24] Recombinant p53 was expressed in *Escherichia coli*, purified from inclusion bodies and refolded as soluble tetrameric protein (Figure 4a).[37] The *in situ* polymerization process using monomers **1** and **2**, as well as crosslinker **3** was optimized to minimize aggregation and precipitation of the soluble p53. A final molar fraction of 1.5% of **2** was used in the monomers, while 5% **3** was added as crosslinkers. We found that p53 concentration must be kept at below 0.7 mg/mL and all steps must be performed in sodium bicarbonate containing buffer to avoid aggregation and precipitation (see Supporting Information). After encapsulation, the azido-functionalized nanocapsules (S-S p53 NC) were buffer-exchanged and concentrated in phosphate-buffered saline. Successful encapsulation was monitored by both DLS and TEM as shown in Figure 4b and Figure 4c, respectively. The native p53 tetramer exhibited hydrodynamic diameter of 7.7±0.5 nm (PDI = 0.27), in line with cryo-EM characterizations.[38,39] Upon encapsulation the average diameter increased to ~27.5±1.0 nm (PDI = 0.39) with a ξ-potential of -0.6mV, and the structural uniformity was observed by Transmission Electron Microscopy (TEM). As a nondegradable control, p53-containing nanocapsules crosslinked with the *N,N'*-methylene bisacrylamide was also prepared. The physical properties of the azido-functionalized non-degradable p53 nanocapsules (ND p53 NC) were nearly identical to that of the S-S p53 NCs.

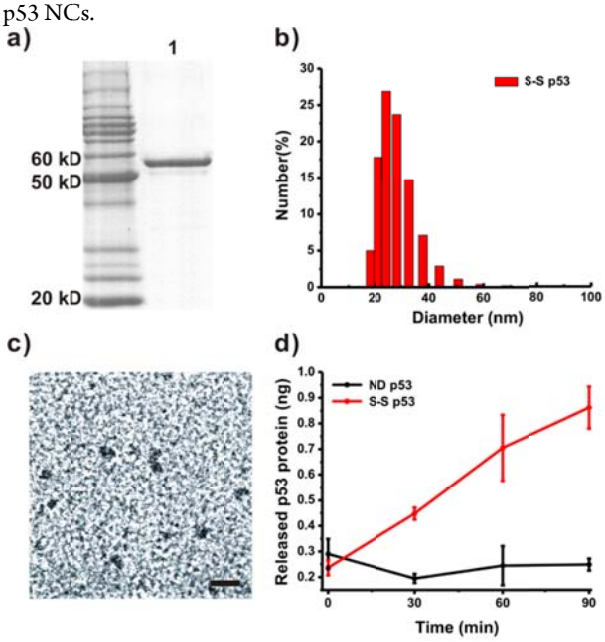

Figure 4. Preparation of recombinant p53 and characterization of LHRH-conjugated p53 nanocapsules. **a**) SDS-PAGE of refolded p53 protein. **b**) The hydrodynamic size distribution of S-S p53 NC as measured by DLS. **c**) TEM image of S-S p53 NC. The scale bar represents 50 nm. **d**) ELISA assay measuring p53 released from S-S p53 NC and ND p53 NC after treatment with 2 mM DTT over 90 min at 37°C (n=2).

To examine the encapsulation effectiveness and redox-sensitive release of the p53 nanocapsules, we performed time-dependent ELISA analysis of p53 nanocapsules both in the presence and absence of the reducing agent DTT (Figure 4d). The ELISA assay employed here requires the p53 to bind to a specific, double stranded target oligonucleotide immobilized on strip well plates. Therefore, encapsulated p53 is physically shielded by the polymer layer and is thus unable to bind to oligonucleotide and to be recognized by the anti-p53 antibody. As expected in the absence of DTT, no native p53 in the solution can be detected within the assay period, indicating the robustness of the polymer layer in both shielding and retaining the p53 cargo. In contrast, the S-S p53 NCs released p53 when 2 mM DTT was added to the nanocapsules, indicating degradation of the crosslinker and release of p53 into the solution. The positive ELISA signal also signifies that the p53 protein subjected to encapsulation and release remained functional. The ND p53 NCs control did not release detectable p53 in the presence of 2 mM DTT, further confirming the redox-responsiveness of the S-S p53 NCs.

Internalization and Release of p53 in cancer cells

To examine the internalization of S-S p53 NCs into cancer cells, we first conjugated the recombinant p53 to rhodamine dye to obtain Rho-p53. Following encapsulation with **1**, **2** and **3** to form rhodamine-labeled NCs, the LHRH peptide **5** was conjugated to the surface using the bifunctional linker **6**. When added to MDA-

MB-231 cells, rhodamine fluorescence can be detected within the cells after a twelve hour incubation period. When analyzed with confocal microscopy, we observed accumulation of Rho-p53 in the nucleus of the targeted cells, which is the expected localization for the transcription factor (Figure 5b). In contrast, no overlap between DAPI and rhodamine fluorescence can be observed when the Rho-p53 was encapsulated in nondegradable linker and internalized. This is consistent with the inability of Rho-p53 to escape the polymer shell in the absence of the redox-sensitive crosslinker **3**. In this case, all the rhodamine signals remained in the cytoplasm (Figure 5a).

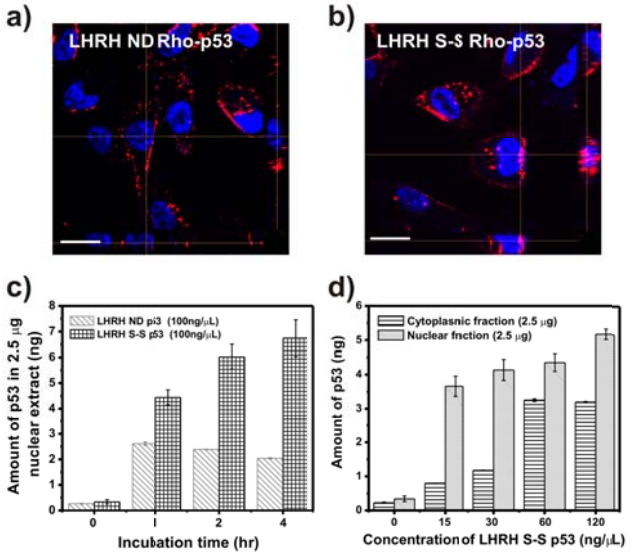

Figure 5. Internalization and location of p53 delivered by designed nanocapsules. Confocal images of MDA-MB-231 cells incubated with 200nM **a**) LHRH-conjugated ND Rho-p53 NC; **b**) LHRH-conjugated S-S Rho-p53 NC; The scale bar represents 20 μm. **c**) ELISA detection of p53 in the nuclear fraction from MDA-MB-231 cells treated with 100 ng/μL LHRH-conjugated ND p53 NC or LHRH-conjugated S-S p53 NC for increasing periods of time; **d**) ELISA detection of p53 in the cytoplasmic and nuclear fraction from MDA-MB-231 cells treated with increasing concentration of LHRH-conjugated S-S p53 NC for one hour.

To further quantify the nuclear localization of delivered p53, we performed the time course ELISA analysis of p53 concentration in both nuclear and cytoplasmic fractions of MDA-MB-231 cells treated with 100 ng/μL of S-S p53 NC or ND p53 NC functionalized with LHRH peptide (Figure 5c). The standard curve relating ELISA signal and p53 level was established using purified recombinant p53. Untreated cells displayed a low level of endogenous p53 (R280K mutant in MDA-MB-231) that is less than 0.5 ng per 2.5 mg of nuclear extract. As shown in Figure 5c, S-S p53 NC treated samples showed a clear accumulation of p53 in the nuclei at time points tested. Close to 7 ng of p53 per 2.5 mg of nuclear extract was observed after four hours. As expected from Rho-p53 localization studies above, significantly higher amounts of p53 can be detected in S-S samples comparing to nondegradable samples. While the ND p53 NC-treated sample showed ~2 ng of nuclei p53 after one hour treatment, no increase was observed after prolonged incubation time. The effect of S-S p53 NC dosage on intracellular p53 concentration was also measured using ELISA. Increasing amount of delivered p53 (from 15 to 120 ng/L) led to increases in both cytoplasmic and nuclear concentration of p53 after one hour (Figure 5d). Therefore, we have shown that LHRH-functionalized, redox- sensitive nanocapsules can effectively deliver recombinant p53 into cancer cells. The delivered and released p53 can dramatically increase the concentration of p53 in both cytoplasm and nuclei. The accumulation in nuclei of cancer cells is especially important, as this is the desired site of action for p53 to reverse cancer cell fate.

Cytotoxicity of p53 Nanocapsules

To examine the effect of delivered p53 on cell viability, we performed cytotoxicity studies using the LHRH-functionalized nanocapsules. Two different versions of p53 were used, the wild type and the tumor selective "super" p53 variant. The super p53 has the gain of function point mutant S121F that has been shown to display more potent apoptotic activity.[40] The mutation alters the specificity of p53 in binding its targets, and in particular, attenuates the activation of MDM2 transcription associated with normal p53 overexpression.[40] The decreased MDM2 feedback control therefore increases apoptosis induction. The S121F mutant kills tumor cells irrespective of p53 status but not wild-type mouse embryo fibroblasts.[40] S-S S121F NCs were prepared in the same manner as S-S p53 NC and conjugated to LHRH peptides using click chemistry. Physical characterizations were performed to verify that the nanocapsules were nearly identical in properties. Both LHRH-conjugated nanocapsules were then added to different cancer cell lines and the cytotoxicity was measured using MTS assay after 48 hours. As shown in Figure 6, LHRH-conjugated S-S p53 NCs showed high selectivity towards MDA-MB-231 cells that overexpresss the LHRH receptor. Nearly no toxicity was observed towards either SK-OV-3 or HFF at 800 nM, the highest concentration assayed. The S121F containing nanocapsules showed potent cytotoxicity, with IC_{50} at ~ 100 nM. In contrast, IC_{50} for the wild type p53 nanocapsules was ~300 nM. We confirmed observed cell death after delivery of S121F is indeed via apoptosis by using TUNEL assay (Figure S7). Negative controls were performed to ensure the observed toxicity is due to the combination of targeted delivery of p53 or tumor selective variant, including i) azido-functionalized S-S S121F NCs not conjugated to LHRH; ii) LHRH conjugated S-S GFP NCs; and iii) azido-functionalized GFP NCs not conjugated to LHRH (Figure S8). In all these controls, the cells remain unaffected by the addition of nanocapsules. These results therefore unequivocally confirm the targeted and functional delivery of p53 can be achieved using the encapsulation and conjugation strategies.

CONCLUSIONS

We developed a new polymerization strategy for the synthesis of protein nanocapsules that display azido functional groups on the surface. By using a cyclooctyne and NHS ester or maleimide containing bifunctional linkers, different targeting ligands such as the LHRH peptide and anti-HER2 scFv can be attached to the surface of the protein nanocapsules. Using GFP as the cargo, we demonstrated the specific internalization of the nanocapsules into cells overexpressing corresponding receptors. Finally, we demonstrated this approach can achieve the functional delivery of the genome guardian p53 protein to trigger apoptosis in targeted cancer cells. LHRH-conjugated nanocapsule can be used as a protein delivery system for the treatment of LHRH receptor overexpressing tumor cells. Our results validate a general approach for targeted protein delivery into tumor cells in a cellular-responsive manner, opening

up new opportunity for the development of protein anticancer treatment.

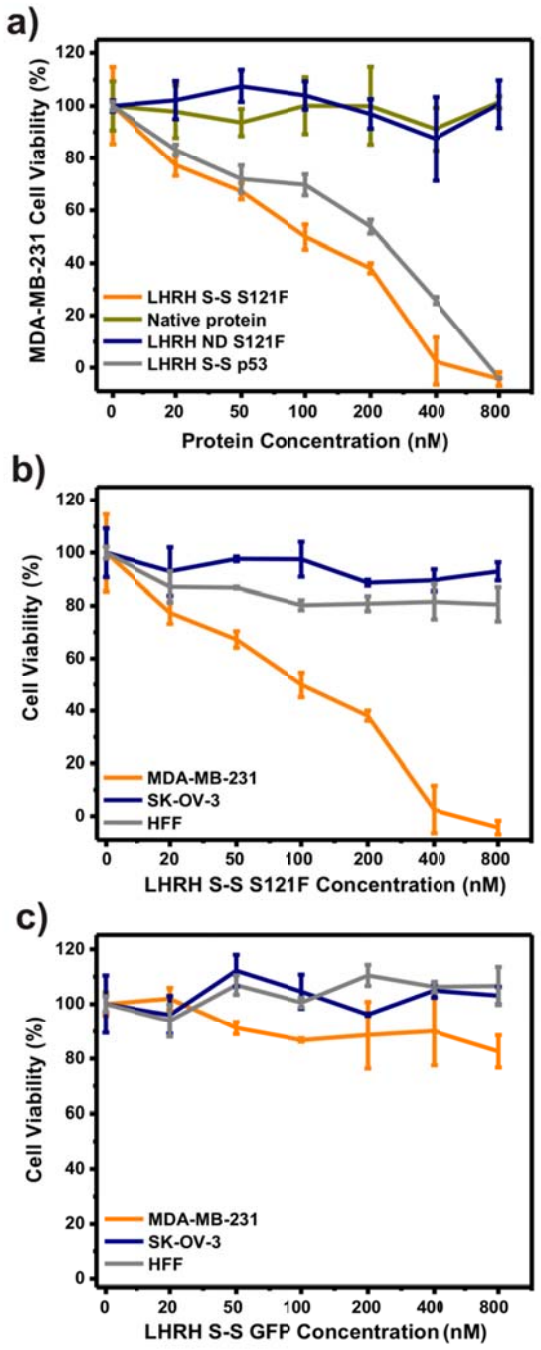

Figure 6. Cytotoxicity of LHRH-conjugated nanocapsules towards cancer cell lines. **a**) MDA-MB-231 cell viability treated with LHRH-conjugated S-S S121F NC, native S121F protein, LHRH-conjugated ND S121F NC, and LHRH-conjugated S-S p53 NC; **b**) MDA-MB-231, SK-OV-3 and HFF treated with LHRH-conjugated S-S S121F NC; **c**) MDA-MB-231, SK-OV-3 and HFF treated with LHRH-conjugated S-S GFP NC.

ASSOCIATED CONTENT

Materials and Methods, experimental details and spectroscopic data. This material is available free of charge via the Internet at http://pubs.acs.org.

AUTHOR INFORMATION

Corresponding Author

* yitang@ucla.edu.

ACKNOWLEDGMENT

This work was supported by a David and Lucile Packard Foundation to Y.T.; a CDMRP BCRP Idea Award BC101380 to Y.T. and P. W.

REFERENCES

(1) Cotter, T. G. *Nat. Rev. Cancer* **2009**, *9*, 501.
(2) Coles, C.; Condie, A.; Chetty, U.; Steel, C. M.; Evans, H. J.; Prosser, J. *Cancer Res.* **1992**, *52*, 5291.
(3) Lacroix, M.; Toillon, R. A.; Leclercq, G. *Endocr. Relat. Cancer* **2006**, *13*, 293.
(4) Blagosklonny, M. V. *Int. J. Cancer* **2002**, *98*, 161.
(5) Senzer, N.; Nemunaitis, J.; Nemunaitis, M.; Lamont, J.; Gore, M.; Gabra, H.; Eeles, R.; Sodha, N.; Lynch, F. J.; Zumstein, L. A.; Menander, K. B.; Sobol, R. E.; Chada, S. *Mol. Cancer. Ther.* **2007**, *6*, 1478.
(6) Issaeva, N.; Bozko, P.; Enge, M.; Protopopova, M.; Verhoef, L. G. G. C.; Masucci, M.; Pramanik, A.; Selivanova, G. *Nat. Med.* **2004**, *10*, 1321.
(7) Vassilev, L. T.; Vu, B. T.; Graves, B.; Carvajal, D.; Podlaski, F.; Filipovic, Z.; Kong, N.; Kammlott, U.; Lukacs, C.; Klein, C.; Fotouhi, N.; Liu, E. A. *Science* **2004**, *303*, 844.
(8) Friedler, A.; Hansson, L. O.; Veprintsev, D. B.; Freund, S. M. V.; Rippin, T. M.; Nikolova, P. V.; Proctor, M. R.; Rudiger, S.; Fersht, A. R. *Proc. Natl. Acad. Sci. U.S.A.* **2002**, *99*, 937.
(9) Lee, Y.; Ishii, T.; Cabral, H.; Kim, H. J.; Seo, J. H.; Nishiyama, N.; Oshima, H.; Osada, K.; Kataoka, K. *Angew. Chem. Int. Edit.* **2009**, *48*, 5309.
(10) Liechty, W. B.; Chen, R. J.; Farzaneh, F.; Tavassoli, M.; Slater, N. K. H. *Adv. Mater.* **2009**, *21*, 3910.
(11) Hu, Y. H.; Atukorale, P. U.; Lu, J. J.; Moon, J. J.; Um, S. H.; Cho, E. C.; Wang, Y.; Chen, J. Z.; Irvine, D. J. *Biomacromolecules* **2009**, *10*, 756.
(12) Giannotti, M. I.; Esteban, O.; Oliva, M.; Garcia-Parajo, M. F.; Sanz, F. *Biomacromolecules* **2011**, *12*, 2524.
(13) Wu, X. J.; Wu, S. Q.; Yang, L.; Han, J. H.; Han, S. F. *J. Mater. Chem.* **2012**, *22*, 17121.
(14) Zheng, C.; Zhang, X. G.; Sun, L.; Zhang, Z. P.; Li, C. X. *J. Mater .Sci.* **2013**, *24*, 931.
(15) Huang, X. L.; Meng, X. W.; Tang, F. Q.; Li, L. L.; Chen, D.; Liu, H. Y.; Zhang, Y. Q.; Ren, J. *Nanotechnology* **2008**, *19*.
(16) Chorny, M.; Hood, E.; Levy, R. J.; Muzykantov, V. R. *J. Control Release* **2010**, *146*, 144.
(17) Cho, M. H.; Lee, E. J.; Son, M.; Lee, J. H.; Yoo, D.; Kim, J. W.; Park, S. W.; Shin, J. S.; Cheon, J. *Nat. Mater.* **2012**, *11*, 1038.
(18) Jiang, T.; Mo, R.; Bellotti, A.; Zhou, J.; Gu, Z. *Adv. Funct. Mater.* **2014**, *24*, 2295.
(19) Gu, Z.; Biswas, A.; Zhao, M. X.; Tang, Y. *Chem. Soc. Rev.* **2011**, *40*, 3638.
(20) Zhao, M. X.; Biswas, A.; Hu, B. L.; Joo, K. I.; Wang, P.; Gu, Z.; Tang, Y. *Biomaterials* **2011**, *32*, 5223.
(21) Zhao, M. X.; Hu, B. L.; Gu, Z.; Joo, K. I.; Wang, P.; Tang, Y. *Nano Today* **2013**, *8*, 11.
(22) Murthy, N., Thng, Y. X. , Schuck, S., Xu, M. C., Fréchet, J. M. *J. Am. Chem. Soc.* **2002**, *124*, 12398.
(23) Murthy, N., Xu, M., Schuck, S., Kunisawa, J., Shastri, N., Fréchet, J. M. *Proc. Natl. Acad. Sci. U.S.A.* **2003**, *100*, 4995.
(24) Bell, S.; Klein, C.; Muller, L.; Hansen, S.; Buchner, J. *J. Mol. Biol.* **2002**, *322*, 917.

(25) Mbua, N. E.; Guo, J.; Wolfert, M. A.; Steet, R.; Boons, G. J. *Chembiochem* **2011**, *12*, 1912.
(26) Ning, X. H.; Guo, J.; Wolfert, M. A.; Boons, G. J. *Angew. Chem. Int. Edit.* **2008**, *47*, 2253.
(27) Baskin, J. M.; Prescher, J. A.; Laughlin, S. T.; Agard, N. J.; Chang, P. V.; Miller, I. A.; Lo, A.; Codelli, J. A.; Bertozzi, C. R. *Proc. Natl. Acad. Sci. U. S. A.* **2007**, *104*, 16793.
(28) Koo, H.; Lee, S.; Na, J. H.; Kim, S. H.; Hahn, S. K.; Choi, K.; Kwon, I. C.; Jeong, S. Y.; Kim, K. *Angew. Chem. Int. Edit.* **2012**, *51*, 11836.
(29) Welser, K.; Perera, M. D. A.; Aylott, J. W.; Chan, W. C. *Chem. Commun.* **2009**, 6601.
(30) Meister, A.; Tate, S. S. *Annu. Rev. Biochem.* **1976**, *45*, 559.
(31) Yan, M.; Du, J.; Gu, Z.; Liang, M.; Hu, Y.; Zhang, W.; Priceman, S.; Wu, L.; Zhou, Z. H.; Liu, Z.; Segura, T.; Tang, Y.; Lu, Y. *Nat. Nanotechnol.* **2010**, *5*, 48.
(32) Nagy, A.; Schally, A. V. *Bio.l Reprod.* **2005**, *73*, 851.
(33) Dharap, S. S.; Wang, Y.; Chandna, P.; Khandare, J. J.; Qiu, B.; Gunaseelan, S.; Sinko, P. J.; Stein, S.; Farmanfarmaian, A.; Minko, T. *Proc. Natl. Acad. Sci. U.S.A.* **2005**, *102*, 12962.
(34) Dharap, S. S.; Qiu, B.; Williams, G. C.; Sinko, P.; Stein, S.; Minko, T. *J. Control Release* **2003**, *91*, 61.
(35) Harris, N.; Dutlow, C.; Eidne, K.; Dong, K. W.; Roberts, J.; Millar, R. *Cancer Res.* **1991**, *51*, 2577.
(36) Dharap, S. S.; Minko, T. *Pharmaceut. Res.* **2003**, *20*, 889.
(37) Bell, S.; Hansen, S.; Buchner, J. *Biophys. Chem.* **2002**, *96*, 243.
(38) Okorokov, A. L.; Sherman, M. B.; Plisson, C.; Grinkevich, V.; Sigmundsson, K.; Selivanova, G.; Milner, J.; Orlova, E. V. *EMBO J.* **2006**, *25*, 5191.
(39) Tidow, H.; Melero, R.; Mylonas, E.; Freund, S. M. V.; Grossmann, J. G.; Carazo, J. M.; Svergun, D. I.; Valle, M.; Fersht, A. R. *Proc. Natl. Acad. Sci. U.S.A.* **2007**, *104*, 12324.
(40) Saller, E.; Tom, E.; Brunori, M.; Otter, M.; Estreicher, A.; Mack, D. H.; Iggo, R. *EMBO J.* **1999**, *18*, 4424.

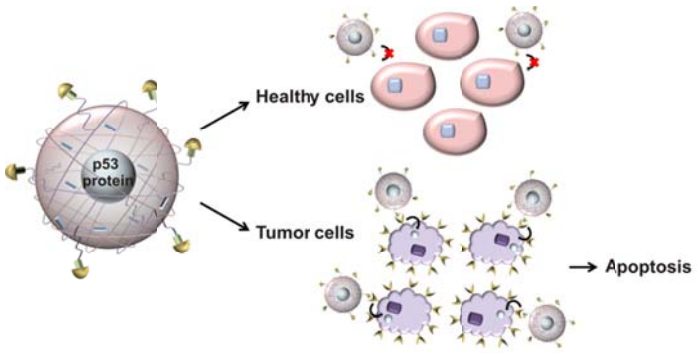
p53
protein
Healthy cells
Tumor cells
Apoptosis